UNIVERSITY OF
Southampton
Institute of Sound and
Vibration Research

ISVR Technical Memorandum

Comparison of Active Structural Acoustic Control on Homogeneous and Composite Sandwich Panels under Deterministic and Stochastic Excitation

J Rohlfing and P Gardonio

ISVR Technical Memorandum No 984
March 2009

SCIENTIFIC PUBLICATIONS BY THE ISVR

Technical Reports are published to promote timely dissemination of research results by ISVR personnel. This medium permits more detailed presentation than is usually acceptable for scientific journals. Responsibility for both the content and any opinions expressed rests entirely with the author(s).

Technical Memoranda are produced to enable the early or preliminary release of information by ISVR personnel where such release is deemed to the appropriate. Information contained in these memoranda may be incomplete, or form part of a continuing programme; this should be borne in mind when using or quoting from these documents.

Contract Reports are produced to record the results of scientific work carried out for sponsors, under contract. The ISVR treats these reports as confidential to sponsors and does not make them available for general circulation. Individual sponsors may, however, authorize subsequent release of the material.

UNIVERSITY OF SOUTHAMPTON

INSTITUTE OF SOUND AND VIBRATION RESEARCH

SIGNAL PROCESSING & CONTROL GROUP

Comparison of Active Structural Acoustic Control on Homogeneous and Composite Sandwich Panels under Deterministic and Stochastic Excitation

by

J Rohlfing and P Gardonio

ISVR Technical Memorandum No. 984

March 2009

Authorized for issue by
Prof R Allen
Group Chairman

Acknowledgement

This research work was supported by a ’Marie Curie Fellowship for Early Stage Research Training’ within the ’European Doctorate Sound and Vibration Studies’ (EDSVS) program.

Contents

List of Tables

List of Figures

Abstract

In this report an element-based model is used to predict the structural response and sound radiation of two smart panels excited by (a) an acoustic plane wave, (b) a stochastic acoustic diffuse field and (c) a turbulent boundary layer. The first panel is made of aluminum, while the second is a composite sandwich panel with equivalent static stiffness but four times lower mass per unit area. The panels are equipped with sixteen decentralised velocity feedback control loops using idealized point force actuators. In contrast to previous studies on smart panels, the analysis is extended to the upper end of the audio frequency range. In this frequency region the response and sound radiation of the panels strongly depend on the spatial characteristics of the excitation field and the sound radiation properties with respect to the bending wavelength on the panels. Considerable reduction in structural response and sound radiation is predicted for the low audio frequency range where the panel response is dominated by well separated resonances of low order structural modes. It is also found that some reduction can be achieved around acoustic and convective coincidence regions, where the coincidence frequencies for the composite sandwich panel are significantly lower than those for the homogeneous aluminium panel.

Nomenclature

Symbol	Description	Unit
Latin Letters:		
a	Modal displacement	
c	Wave speed	m/s
d	Distance between the sandwich faceplate neutral axis	m
f_1	Frequency	Hz
f_2	Force	N
h	Thickness (panel)	m
j	Imaginary unit defined as: $j = \sqrt{-1}$	
k	Wavenumber	rad/m
l	length	m
m	Mode order x-direction	
n	Mode order y-direction	
p	Acoustic Pressure	N/m^2
t	Time	s
w	Transverse displacement	m
x	x-coordinate (plate axis)	m
y	y-coordinate (plate axis)	m
z	z-coordinate (perpendicular to plate)	m
A	Area	m^2
D	Flexural rigidity or bending stiffness	Nm^2
E_1	Young's modulus of elasticity	N/m^2
E_2	Kinetic Energy	J

F	Modal force or generalised force	N
H	Control gain	
I	Second moment of area	m^4
L	Correlation length	m
M	Mass (total / modal / elemental)	Kg
N	Total number (modes / elements)	
P	Power	W
R	Distance between two points on the panel	
S	Spectral density	
U	Speed	m/s
Y	Mobility	m/(Ns)
Z	Impedance	Ns/m
$\mathbf{A}$	Power transfer Matrix	
$\mathbf{F}$	Force Matrix (modal and elemental)	
$\mathbf{G}$	Mobility matrix including velocity feedback control	

Greek Letters:

η	Damping loss factor	
θ	Angle of incidence angle relative to surface normal	rad or deg
ν	Poisson's ratio	
ρ	Material density	kg/m^3
ϕ	Natural modes or modeshapes	
φ	Angle of incidence relative to x axis	rad or deg
ω	Rotational frequency	rad/s
$\mathbf{\Omega}$	Matrix of modal resonant terms	

Subscripts

0	Property of air
c_1	Control element
c_2	Critical
c_3	Specific to the sandwich core
$conv.$	Convection

e	Plate element (element centre point)
f	Specific to faceplate
i	Index (plate elements)
j	Index (plate elements)
n	mode order
r	Index (modes)
rad	Radiation
s_1	Index (modes)
s_2	Corresponding to shear
ADF	Specific to Acoustic diffuse field
TBL	Specific Turbulent boundary layer

Mathematical:

X	Real value X
$\tilde{X}$	Complex Value X
$Re\{\tilde{X}\}$	Real part of X
$Im\{\tilde{X}\}$	Imaginary part of X
$\hat{X}$	Peak value X
$\tilde{X}^*$	Conjugant of X
$E\left[\tilde{X}^*\tilde{X}\right]$	Expectation of $\left[\tilde{X}^*\tilde{X}\right]$ for infinite sampling length
$\mathbf{var}\left[X\right]$	variance of X
X^n	X to the power of n
$\exp(X)$	e to the power of X
$\dot{X}$	First derivative of X in respect to time
$\mathbf{X}$	Matrix X
$\mathbf{X^{-1}}$	Inverse of Matrix X
$\mathbf{X^T}$	Non conjugate transpose of Matrix X
$\mathbf{X^H}$	Complex conjugate transpose (Hermitian transpose) of Matrix X
$\mathbf{I}$	Identity matrix

Chapter 1

Introduction

Environmental and economic considerations increase the demand for weight-optimized structural design. This often conflicts with the requirements for noise control and acoustical comfort. Various active control approaches have been shown to enhance the sound attenuation through a panel at low frequencies where the structural response is dominated by discrete resonant modes with low modal overlap. Very appealing approaches are those of active structural acoustic control (ASAC) and active vibration control (AVC) where actuators and sensors are integrated within the structure to create 'smart panels' [1 - 17]

For many practical vibro-acoustic problems, the excitation is not deterministic. Common examples of stochastic excitations are diffuse acoustic sound fields (ADF) [18] or turbulent boundary layers (TBL) [19, 20], which are often encountered in transportation vehicles such as aircraft, high speed trains and cars [21, 22]. These disturbances can be described by analytical formulations for the statistical properties of the resulting excitation field on a panel surface. An important characteristic of such disturbances is the projection of periodic pressure fluctuations onto the panel surface. In the case of acoustic disturbances this depends on the acoustic wavelength and angle of incidence [3]; for a TBL disturbance this depends on the convective wavelength and the direction of the flow [19, 23]. Frequencies at which the convective or acoustic wavelength are the same as the transverse wavelength on a structure are known as coincidence frequencies. Coupling between excitation wavelengths, transverse structural wavelength and acoustic wavelength have a significant influence on the sound transmission through a partition. For thin aluminum panels, the acoustic coincidence frequency falls into the upper end of the audio

frequency range. The convective coincidence frequency is typically much lower and affects the panel response in the mid audio frequency range. Composite sandwich panels feature a high stiffness to mass ratio and therefore become increasingly popular in the design of lightweight vehicles. However, for stiff lightweight sandwich panels the convective and acoustic coincidence shifts towards lower frequencies and may cause noise transmission problems.

The objective of this report is twofold. Firstly, to investigate and contrast the structural response and the sound radiation in the audio frequency range produced by homogeneous and lightweight sandwich panels subject to deterministic and stochastic distributed excitations. Secondly, to study and compare the control effects produced by an array of idealized velocity feedback control loops on homogeneous and lightweight sandwich panels.

An element approach [4, 24, 25] is used to predict the structural response and sound radiation of the two smart panels excited by (a) an acoustic plane wave, (b) a stochastic acoustic diffuse field and (c) a turbulent boundary layer. The first panel is made of aluminum while the second is a composite sandwich panel with equivalent static stiffness but four times lower mass per unit area. The panels are equipped with sixteen decentralised velocity feedback control loops using idealized point force actuators and collocated idealized velocity sensors so that the control loops are bound to be unconditionally stable. [4, 26]. In this way the intrinsic characteristics of the decentralised feedback control system are investigated independently from the stability limits of the control units due to the electrodynamic responses of the sensor actuator pairs. In contrast to previous studies on smart panels, the analysis is extended to the upper end of the audio frequency range to include the acoustic coincidence frequency region.

The first part of this report covers the element based model for the structural response and radiated sound power for a thin homogeneous panel and a sandwich panel under deterministic and stochastic excitations. The model is then used to predict the panel kinetic energy and radiated sound power for the two panels without control. Finally the results for the structural response and radiated sound power of the two panels with decentralised velocity feedback control are presented. The derivation of the stochastic excitation model from first principles and resulting matrix formulations are discussed in Appendix A.

Chapter 2

Panel model

The steady state flexural response and sound radiation of a smart aluminium panel and a smart composite sandwich panel are modelled using an elemental approach [4, 24, 25]. Figure 2.1 shows the geometry of the panels, which are simply supported in an infinite baffle. They are equipped with sixteen decentralized ideal velocity sensor and actuator pairs to illustrate the effects of decentralized velocity feedback control. On the source side the panels are exposed to a surface pressure fluctuation induced by different types of deterministic and stochastic disturbances. On the receiver side the panels are radiating into an infinite half space. The geometrical and physical parameters of the panel models are summarized in Table 2.1 and Table 2.2. The physical parameters of the surrounding media on source and receiving side of the panel is chosen as that of air with a mass density ρ = 1.21 kgm^{-3} and characteristic sound speed c_0 = 343 ms^{-1}. The model is weakly coupled, fluid loading effects and radiation losses have been neglected. This is a reasonable assumption for excitation and radiation into air. The effects of fluid loading and flexible boundaries are discussed in Reference [27].

The steady state response is derived assuming time-harmonic excitation of the form $Re\{\exp(j\omega t)\}$ where ω is the angular frequency and $j = \sqrt{-1}$. For brevity the time-harmonic term $\exp(j\omega t)$ will be omitted in the formulation which will be given in complex form. Therefore, the time harmonic velocity $\dot{w}(t) = Re\{\tilde{\dot{w}}\exp(j\omega t)\}$ and force $F(t) = Re\{\tilde{F}\exp(j\omega t)\}$ fluctuations will be replaced by the complex velocity and force phasor $\tilde{\dot{w}}$ and $\tilde{F}$ respectively. Throughout the report $\tilde{}$ will be used to identify complex, frequency dependent functions. As shown in Figure 2.1(a), the panel is sub-

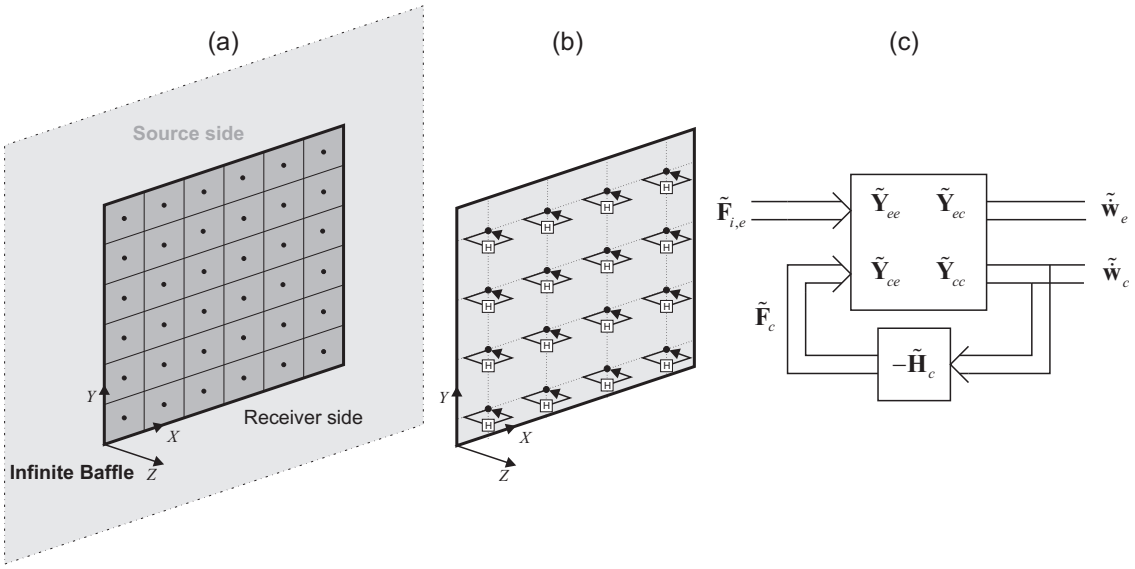

Figure 2.1: Schematic of the panel model. (a) Panel in infinite baffle subdivided into a grid of elements, (b) Panel with 16 direct velocity feedback loops, (c) "two port" block diagram for panel model with decentralised multi channel feedback control.

divided in a grid of elements so that the excitation forces and velocity response of the panel are determined at the element centre coordinates. As shown in Figure 2.1(b), the decentralised feedback control system is formed by a 4×4 grid of velocity feedback loops using collocated and dual point velocity sensor and point force actuators. The closed loop response of the panel can be modelled with the two ports block diagram in Figure 2.1(c), which, assuming the system is linear, indicates that both the response at the elements centres and the control positions result from the linear superposition of the vibration induced by the primary excitation, produced by the pressure field over the surface on the source side of the panel, and the secondary excitation produced by the control point forces, which depends on the control velocities via the feedback control gains. Thus the velocity response at the centres of the panel elements is given by

$$\dot{\tilde{\mathbf{w}}}_e = \tilde{\mathbf{Y}}_{ee}\tilde{\mathbf{F}}_e + \tilde{\mathbf{Y}}_{ec}\tilde{\mathbf{F}}_c, \tag{2.1}$$

where $\dot{\tilde{\mathbf{w}}}_e = [\dot{\tilde{w}}_{e_1}, \dot{\tilde{w}}_{e_2}, ..., \dot{\tilde{w}}_{e_{N_e}}]^T$ is the $[N_e \times 1]$ dimensional vector of complex element velocities, $\tilde{\mathbf{F}}_e = [\tilde{F}_{e_1}, \tilde{F}_{e_2}, ..., \tilde{F}_{e_{N_e}}]^T$ is the $[N_e \times 1]$ dimensional vector of excitation forces due to the pressure field incident on the source side of the elements, $\tilde{\mathbf{F}}_c = [\tilde{F}_{c_1}, \tilde{F}_{c_2}, ..., \tilde{F}_{c_{N_c}}]^T$ is the $[N_c \times 1]$ dimensional vector of feedback control forces, $\tilde{\mathbf{Y}}_{ee}$ is the $[N_e \times N_e]$ dimensional matrix of element centre point and transfer mobilities

and $\tilde{\mathbf{Y}}_{ec}$ is the $[N_e \times N_c]$ dimensional matrix of transfer mobilities from the control locations to the panel element centres. The mobility functions in the matrices $\tilde{\mathbf{Y}}_{ee}$ and $\tilde{\mathbf{Y}}_{ec}$ have been derived with the following modal summation formula

$$\tilde{Y}_{i,j} = j\omega \sum_{r=1}^{N} \frac{\phi_r\left(x_i, y_i\right)\ \phi_r\left(x_j, y_j\right)}{M\ \omega_r^2\left(1 + j\eta\right) - \omega^2}, \tag{2.2}$$

where ϕ_r is the r-th mass-normalised natural mode of the panel, ω_r is the r-th natural frequency and ω is the observation frequency. $M = l_x l_y \rho h$ is the total mass of the panel, where l_x and l_y are the panel dimensions, h is the panel thickness and ρ is the density of the panel material. The coordinates (x_i, y_i) and (x_j, y_j) identify the centre positions of the elements i and j on the panel surface. As shown in the block diagram in Figure 2.1(c), for direct velocity feedback control, the vector of control forces is given by

$$\tilde{\mathbf{F}}_c = -\tilde{\mathbf{H}}_c \tilde{\dot{\mathbf{w}}}_c, \tag{2.3}$$

where $\tilde{\mathbf{H}}_c$ is the $[N_c \times N_c]$ dimensional diagonal matrix of control gains and $\tilde{\dot{\mathbf{w}}}_c = [\tilde{\dot{w}}_{c_1}, \tilde{\dot{w}}_{c_2}, ..., \tilde{\dot{w}}_{c_{N_c}}]^T$ is the $[N_c \times 1]$ dimensional vector of velocity sensor outputs at the control locations. According to the "two port" block diagram in Figure 2.1(c), the vector of control point velocities is given by

$$\tilde{\dot{\mathbf{w}}}_c = \tilde{\mathbf{Y}}_{ce} \tilde{\mathbf{F}}_e + \tilde{\mathbf{Y}}_{cc} \tilde{\mathbf{F}}_c, \tag{2.4}$$

where $\tilde{\mathbf{Y}}_{cc}$ is the $[N_c \times N_c]$ dimensional matrix of point and transfer mobilities at the control locations. Substituting Equation (2.3) into Equation (2.4) gives

$$\tilde{\dot{\mathbf{w}}}_c = \tilde{\mathbf{Y}}_{ce} \tilde{\mathbf{F}}_e - \tilde{\mathbf{Y}}_{cc} \tilde{\mathbf{H}}_c \tilde{\dot{\mathbf{w}}}_c. \tag{2.5}$$

An explicit formulation for $\tilde{\dot{\mathbf{w}}}_c$ can hence be derived as

$$\tilde{\dot{\mathbf{w}}}_c = \left(\mathbf{I}_c + \tilde{\mathbf{Y}}_{cc} \tilde{\mathbf{H}}_c\right)^{-1} \tilde{\mathbf{Y}}_{ce} \tilde{\mathbf{F}}_e. \tag{2.6}$$

The control force $\tilde{\mathbf{F}}_c$ in Equation (2.3) can subsequently be reformulated to yield

$$\tilde{\mathbf{F}}_c = -\tilde{\mathbf{H}}_c \left(\mathbf{I}_c + \tilde{\mathbf{Y}}_{cc} \tilde{\mathbf{H}}_c \right)^{-1} \tilde{\mathbf{Y}}_{ce} \tilde{\mathbf{F}}_e. \tag{2.7}$$

Substituting Equation (2.7) into Equation (2.1) and rearranging for $\tilde{\dot{\mathbf{w}}}_e$ finally gives the vector of element velocities as

$$\tilde{\dot{\mathbf{w}}}_e = \left[\tilde{\mathbf{Y}}_{ee} - \tilde{\mathbf{Y}}_{ec} \tilde{\mathbf{H}}_c \left(\mathbf{I}_c + \tilde{\mathbf{Y}}_{cc} \tilde{\mathbf{H}}_c \right)^{-1} \tilde{\mathbf{Y}}_{ce} \right] \tilde{\mathbf{F}}_e = \tilde{\mathbf{G}}_{ee} \tilde{\mathbf{F}}_e, \tag{2.8}$$

where $\tilde{\mathbf{G}}_{ee} = \tilde{\mathbf{Y}}_{ee} - \tilde{\mathbf{Y}}_{ec} \tilde{\mathbf{H}}_c (\mathbf{I}_c + \tilde{\mathbf{Y}}_{cc} \tilde{\mathbf{H}}_c)^{-1} \tilde{\mathbf{Y}}_{ce}$ is the panel element mobility matrix with active control.

2.1 Aluminium panel

The Aluminium panel has been modelled as a thin homogenous and isotropic plate with all sides simply supported. The mass-normalised mode shapes are given by [3]

$$\phi_r(x, y) = 2 \sin \left(\frac{m_r \, \pi x}{l_x} \right) \sin \left(\frac{n_r \, \pi y}{l_y} \right), \tag{2.9}$$

where and m_r and n_r are the the mode orders of mode r in the x- and y-direction of the panel. The natural frequencies result from

$$\omega_r = \sqrt{\frac{D}{\rho h}} \left[\left(\frac{m_r \, \pi}{l_x} \right)^2 + \left(\frac{n_r \, \pi}{l_y} \right)^2 \right], \tag{2.10}$$

where ρh is the panel mass per unit area, $D = EI/(1 - \nu^2)$ is the bending stiffness $I = h^3/12$ is the area moment of the cross section. Also E is the Young's modulus of elasticity and ν is the Poisson's ratio of the panel material. The panel geometry and material properties are given in Table 2.1.

Table 2.1: Geometry and physical properties for a homogeneous aluminium panel.

Parameter	Symbol	Value	Unit
x-Dimension	l_x	278	mm
y-Dimension	l_y	247	mm
Thickness	h	1.6	mm
Mass density	ρ	2720	kg m^{-3}
Young's Modulus	E	70	GPa
Poisson's ratio	ν	0.33	–
Modal loss factor	η	0.02	–

2.2 Composite sandwich panel

The dynamic response of the composite sandwich panel is modelled using a basic theory [3, 28] which considers pure bending of the cross-section and the faceplates and pure transverse shear of the core. The panel is assumed to have the same material properties in x- and y-direction. The relationship between the transverse wavenumber k and the wavenumbers corresponding to pure bending and to pure shear of a sandwich panel is given by

$$1 + \left(\frac{k_s}{k_b}\right)^2 \left(\frac{k}{k_b}\right)^2 - \left(\frac{k}{k_b}\right)^4 - \left(\frac{k_b}{k_{bf}}\right)^4 \left(\frac{k_s}{k_b}\right)^2 \left(\frac{k}{k_b}\right)^6 = 0, \tag{2.11}$$

where k_s is the shear wavenumber in the absence of transverse bending forces, k_b is the overall cross-section bending wavenumber in the absence of shear distortion and k_{bf} is the bending wavenumber for faceplate bending alone. These wavenumbers are given as

$$\text{(a)}\ k_s^2 = \frac{m''\omega^2}{G\,d}, \qquad \text{(b)}\ k_b^4 = \frac{m''\omega^2}{D_1}, \qquad \text{(c)}\ k_{bf}^4 = \frac{m''\omega^2}{2\,D_2}, \tag{2.12}$$

where m'' is the total mass of the panel per unit area, G is the core shear modulus and, as shown in Figure 2.2, d is the distance between the faceplates neutral axis. Also D_1 is the bending stiffness of the cross-section and D_2 is the bending stiffness of a individual faceplate. These flexural stiffness terms are given by

$$\text{(a)}\ D_1 = \frac{E d^2 h_f}{2\,(1-\nu^2)}, \qquad \text{(b)}\ D_2 = \frac{E h_f^3}{12\,(1-\nu^2)}. \tag{2.13}$$

The physical parameters used to model the composite sandwich panel are given in Table 2.2. The parameters are chosen to yield a panel with equal static stiffness but a four times lower mass per unit area than that of the homogeneous 1.6 mm thick aluminium panel. Equation (2.11) has one real and two imaginary pairs of axis symmetric solutions. For simplicity the sandwich panel is assumed to have the same mode shapes as a corresponding thin simply supported panel given in Equation (2.9) and that (a) the equivalent flexural rigidity D, (b) wavenumber k_r and (c) natural frequencies ω_r are given by

$$\text{(a) } D = \frac{\omega^2\, m''}{k^4}, \quad \text{(b) } k_r = \sqrt{\left(\frac{m_r \pi}{l_x}\right) + \left(\frac{n_r\, \pi}{l_y}\right)}, \quad \text{(c) } \omega_r = \sqrt{\frac{k_r^4 \frac{D_1}{m''} + k_r^6 \frac{2 D_2 D_1}{G\, d\, m''}}{1 + k_r^2 \frac{D_1}{G\, d}}}, \tag{2.14}$$

where the wavenumber k in Equation (2.14)(a) corresponds to the real wavenumber solution of Equation (2.12), which corresponds to travelling waves. The imaginary wavenumber solutions to Equation (2.11) correspond to decaying near fields waves, which are neglected. The highest mode order of interest is calculated using the equivalent flexural rigidity at the highest frequency of interest. The acoustic coincidence frequency is found by reformulating Equation (2.11) as an implicit function in ω_c. Setting $\omega = \omega_c$ and $k = k_c = \omega_c / c_0$ Equation (2.11) results in the following relationship

$$\omega_c^4 \left(\frac{2 D_2 D_1}{G\, d\, m'' c_0^6}\right) + \left(\frac{D_1}{m'' c_0^4} - \frac{D_1}{G\, d\, c_0^2}\right) - 1 = 0. \tag{2.15}$$

This basic model captures the principal characteristics of a sandwich panel and is thought to be suitable for an initial comparison between the structural response and radiated sound power of thin homogeneous and sandwich active panels. A More complex model, considering near field waves and the cross-section dynamics of the sandwich structure, may be needed for further, more detailed investigations. In particular, the near field wave effect should play an important role in the stability of the feedback control loops when realistic sensor and actuator transducers are considered.

Table 2.2: Cross section geometry and physical properties for the composite sandwich panel.

Parameter	Symbol	Value	Unit
Thickness of face plate	h_f	0.3	mm
Core depth	d	3	mm
Mass density face plates	ρ_f	1000	kg m^{-3}
Mass density core	ρ_c	180	kg m^{-3}
Panel mass per unit area[1]	m''	1.086	kg m^{-2}
Young's modulus face plates	E	17.7	GPa
Poisson's ratio	ν	0.33	–
Shear modulus core	G	80	MPa
Loss factor	η	0.02	–

[1] $m'' = 2h_f\rho_f + (d - h_f)\rho_c$

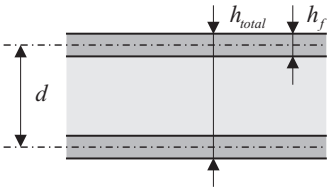

Figure 2.2: Sketch of sandwich panel cross section geometry.

Chapter 3

Excitation models

3.1 Acoustic plane wave

Acoustic plane waves are an example of distributed, deterministic disturbance. An acoustic plane wave excitation is characterised by its sound pressure amplitude and its angels of incidence θ, measured from the z-axis, normal to the panel and the angle φ, in the x-y-plane, measured from the x-axis. Assuming time harmonic pressure fluctuations, the incident sound pressure acting on the source side of the panel is given as

$$p(x, y, t) = Re\left\{\tilde{p}(\omega)e^{j(\omega t - k_x x - k_y y)}\right\}, \tag{3.1}$$

where $\tilde{p}(\omega)$ is the pressure phasor of the incident wave. The wavenumbers in x and y directions are given by

$$\text{(a)}\ \ k_x(\omega) = k_0(\omega)\sin\theta\cos\varphi, \qquad \text{(b)}\ \ k_y(\omega) = k_0(\omega)\sin\theta\sin\varphi, \tag{3.2}$$

where $k_0 = \omega/c_0$ is the acoustic wavenumber and c_0 is the speed of sound in air as specified in Section 2. The pressure excitation on a single panel element is approximated as a point force acting on the element centre,

$$\tilde{F}_{e_i}(\omega) = 2\,A_e\hat{p}(\omega)e^{-j(k_x x_i + k_y y_i)}, \tag{3.3}$$

where A_e is the area of an element and the factor two accounts for the assumption of blocked forces on the panel surface which causes a doubling of pressure. The incident forces for all elements are cast into a $[Ne \times 1]$ dimensional vector which is then used as the excitation term in Equation (2.8).

3.1.1 Panel kinetic energy

The response of the panel is assessed in terms of it's total kinetic energy, which gives an indicator of the spatially averaged vibration and also of the near field sound radiation. For harmonic excitations, the time-averaged kinetic energy of a thin rectangular panel with uniform mass per unit area is given by [3]

$$E(\omega) = \frac{\rho h}{4} \int_0^{l_x} \int_0^{l_y} \left| \tilde{\dot{w}}(x, y, \omega) \right|^2 \, dx \, dy, \tag{3.4}$$

where the additional factor 1/2 arises from the conversion from peak to RMS values. In the elemental approach the surface integral in Equation (3.4) is substituted by a sum over the element velocities [3]. Utilizing matrix algebra this summation can be calculated from the inner Hermitian product of the element velocity vectors. This yields the total kinetic energy as [see Appendix A Equations (A.21) to (A.32)]

$$E(\omega) = \frac{M_e}{4} \; \tilde{\dot{\mathbf{w}}}_e^H(\omega) \tilde{\dot{\mathbf{w}}}_e(\omega), \tag{3.5}$$

where ^{H} denotes the Hermitian transpose and M_e is the mass of an individual panel element.

3.1.2 Radiated sound power

The sound radiation by the panel is expressed in terms of the total sound power radiation which gives an indication of the far field, spatially averaged, sound radiation. The time averaged far field total sound power radiated on one side of the panel is given by [3]

$$P(\omega) = \frac{1}{2} \int_0^{l_x} \int_0^{l_y} Re \left\{ \tilde{\dot{w}}^*(x, y, \omega)\, p(x, y, \omega) \right\} dx\, dy, \tag{3.6}$$

where * denotes the complex conjugate and the factor 1/2 arises from the conversion from peak to RMS values. Considering radiation into free space, for an ideally planar panel, the Rayleigh integral [3] is used to rewrite the acoustic pressure on the surface in terms of the surface velocities and radiation impedance. Utilizing matrix algebra Equation (3.6) can be cast in the form [see Appendix A Equations (A.33) to (A.42)]

$$P(\omega) = \tilde{\dot{\mathbf{w}}}_e^H(\omega) \mathbf{R}_{rad}(\omega) \tilde{\dot{\mathbf{w}}}_e(\omega), \tag{3.7}$$

where $\mathbf{R}_{rad}(\omega)$ is the $[N_e, N_e]$ dimensional radiation matrix with the elements [see Appendix A Equations (A.43) to (A.46)]

$$R_{rad_{i,j}} = \frac{\omega^2 \rho_0 A_e^2}{4\pi c_0} \frac{\sin(k_0 R_{i,j})}{k_0 R_{i,j}}. \tag{3.8}$$

In this equation k_0 is the acoustic wavenumber on the receiving side of the panel and $R_{i,j} = \sqrt{(x_i - x_j)^2 + (y_i - y_j)^2}$ is the distance between the centres of the elements i and j. The distance $R_{i,i}$ is zero, thus the radiation terms $\tilde{R}_{rad_{i,i}}$ on the main diagonal of the radiation matrix are undefined. However, using L' Hôpital's rule [29] it is found that

$$\lim_{R \to 0} \frac{\sin(k_0 R)}{k_0 R} = \lim_{R \to 0} \frac{k_0 \cos(k_0 R)}{k_0} = 1. \tag{3.9}$$

3.2 Stochastic excitation

For many practical vibro-acoustic problems, the excitation is not deterministic. For instance acoustic diffuse sound fields (ADF) or turbulent boundary layer (TBL) pressure fields produced by the interaction of a turbulent flow of fluid and a structure, are often encountered in transportation vehicles such as aircraft, high speed trains and cars. Analytical formulations for the statistical properties of the excitation fields produced by ADF and TBL have been derived. These formulations describe disturbances in terms of power

spectral density and spatial correlation functions. The response and sound radiation induced by such random excitation fields are also expressed in terms of power spectral densities. In particular the response is expressed in terms of the power spectral density for the total kinetic energy, which for a panel structure, is given by [see Appendix A Equations (A.47) to (A.49)]

$$S_E(\omega) = \frac{\rho h}{2} \int_0^{l_x} \int_0^{l_y} \lim_{T\to\infty} E\left[\frac{1}{T}\tilde{\dot{w}}^*(x,y,\omega)\tilde{\dot{w}}(x,y,\omega)\right] dx\, dy, \tag{3.10}$$

Considering the formulation for the elemental approach presented in Section 2, Equation (3.10) can be reformulated to give [compare Appendix A Equations (A.49) to (A.63)]

$$S_E(\omega) = \frac{M_e}{2}\ trace\left(\tilde{\mathbf{G}}_{ee}^H\, \tilde{\mathbf{S}}_{f_e f_e}(\omega)\, \tilde{\mathbf{G}}_{ee}\right). \tag{3.11}$$

where $\tilde{\mathbf{S}}_{f_e f_e}$ is the $[N_e \times N_e]$ dimensional matrix of cross spectral densities between the centres of panel elements and $\tilde{\mathbf{G}}_{ee}$ is the panel element point and transfer mobility matrix with active control as defined in Equation (2.8). The matrix of cross spectral densities of the elemental excitation due to a time and spatial stochastic disturbance has the form

$$\tilde{\mathbf{S}}_{f_e f_e}(\omega) = A_e^2\, \Psi(\omega)\, \tilde{\mathbf{C}}_{ee}(\omega), \tag{3.12}$$

where A_e is the arear of an element, $\Psi(\omega)$ is the time averaged power spectrum of the disturbance per unit area and $\tilde{\mathbf{C}}_{ee}$ is the $[N_e \times N_e]$ dimensional spatial cross correlation matrix of the excitation forces calculated at the element centre locations. The sound radiation is expressed in terms of the power spectral density of the radiated sound power into an infinite half space on the receiving side of the panel, which is given by

$$S_P(\omega) = Re\left\{\int_0^{l_x} \int_0^{l_y} \lim_{T\to\infty} E\left[\frac{1}{T}\tilde{\dot{w}}^*(x,y,\omega)\tilde{p}(x,y,0,\omega)\right] dx\, dy\right\}. \tag{3.13}$$

Considering the elemental formulation Equation (3.13) can be reformulated to give [see Appendix A Equations (A.64) to (A.72)]

$$S_{PP}(\omega) = 2\,trace\left[\left(\tilde{\mathbf{G}}_{ee}^{H}\,\tilde{\mathbf{S}}_{f_e f_e}\,\tilde{\mathbf{G}}_{ee}\right)\mathbf{R}_{rad}\right], \tag{3.14}$$

where $\mathbf{R}_{rad}$ is the element radiation resistance matrix as defined in Equation (3.8).

3.2.1 Acoustic diffuse field

Acoustic diffuse field is a widely used model to describe the excitation produced by random acoustic plane waves incident to a surface for all angles. The cross spectral density for an acoustic diffuse field excitation has been discussed by Shorter and Langley [30]. The power spectral density of an acoustic diffuse field is given by

$$\Psi_{ADF}(\omega) = 4E\left[\tilde{p}\,\tilde{p}^{*}\right] = 4\langle\overline{\tilde{p}^{2}}\rangle \tag{3.15}$$

where $\tilde{p}$ denotes the complex acoustic pressure. The factor 4 arises from the pressure doubling across a rigid surface and from the relationship between the pressure magnitude and mean square value. The spatial correlation function for an acoustic diffuse field on the surface of a rigid infinite plane is given by [30]

$$C_{ADF_{i,j}}(\omega) = \frac{\sin\left(k_0\,R_{i,j}\right)}{k_0\,R_{i,j}}, \tag{3.16}$$

where k_0 is the acoustic wavenumber on the source side of the panel and $R_{i,j}$ is the distance between the centres of the elements i and j. It is interesting to note that the correlation function for an ADF disturbance has the same spatial characteristics as the Radiation matrix in Equation (3.8).

3.2.2 Turbulent Boundary Layer

Turbulent boundary layer disturbance models are widely used to describe the excitation produced on a surface by a turbulent fluid flow. Models for the spatial correlation of turbulent boundary layer disturbances have been discussed in References [25] and [31]. The most common expression for TBL cross spectral density is given by Corcos [32].

The parameters that define the model of the spatial correlation of a fully developed TBL on the smart panels considered in this study, are given in Table 3.1. The flow direction is parallel to the y-axis. The spatial correlation function in x-direction (span wise) and y-direction (stream wise) is given by

$$\tilde{C}_{TBL_{i,j}}(\omega) = \exp\left(-\frac{|R_{x_{i,j}}|}{L_x(\omega)}\right) \exp\left(-\frac{|R_{y_{i,j}}|}{L_y(\omega)}\right) \exp\left(\frac{-j\omega R_{y_{i,j}}}{U_c}\right), \tag{3.17}$$

where $|R_{x_{i,j}}| = |x_i - x_j|$ and $|R_{y_{i,j}}| = |y_i - y_j|$ are the distance between the centres of element i and j in x- and y-direction and L_x and L_y are the correlation lengths in x and y, given by

$$\text{(a)}\ \ L_x(\omega) = \frac{\alpha_x U_{conv.}}{\omega}, \qquad \text{(b)}\ \ L_y(\omega) = \frac{\alpha_y U_{conv.}}{\omega}, \tag{3.18}$$

where α_x and α_y are empirical constants taken from [25, 31] and $U_{conv.}$ is the convection velocity. The convection velocity is a function of frequency [32, 23], but can be approximated as a fixed fraction of the free flow velocity. Since this assumes that the cross correlation function is independent from the boundary layer thickness, it overestimates the correlation length at very low frequency. A comprehensive review on TBL excitation models is given by Cousin [23]. In general, the power spectral density of the surface pressure fluctuations due to turbulent boundary layer decreases with increasing frequency. The results presented in this report do not reflect this dependency but only compare the panel response to different disturbances with respect to their frequency dependent spatial correlation.

Table 3.1: Parameters for the Turbulent boundary layer disturbance.

Parameter	Symbol	Value	Unit
Free-stream velocity	U_∞	225	m/s
Convection velocity	$U_{conv.}$	0.6 $\times U_\infty$	m/s
Empirical constant [1]	α_x	1.2	–
Empirical constant [1]	α_y	8	–

[1] taken from Ref. [25]

3.3 Element Resolution

The required element grid density depends on (a) the disturbance characteristics, (b) the flexural response of the panel and (c) the radiation properties of the panels, which are given by the radiation matrix. For frequencies below the convective and acoustic coincidence frequencies the bending wavelength is shorter than the acoustic wavelength; thus the required mesh density is determined by the bending wave length $\lambda_b = c_b(f)/f$ on the panels. For frequencies above the acoustic coincidence frequency, it is the acoustic wavelength that is shorter than the bending wavelength on the panel; therefore the element density is determined by the acoustic wavelength $\lambda_0 = c_0/f$. For TBL disturbance, the element density in the stream-wise direction for frequencies above the convective coincidence is determined by the convective wavelength $\lambda_{conv.} = U_{conv.}/f$. In the span-wise x-direction the correlation function in (3.17) is exponentially decaying, thus a low resolution of the elements grid in x-direction results an overestimation of the structural response but does not change its general characteristics. In general at least two elements per shortest wavelength are required to avoid spatial aliasing. Numerical convergence studies showed that 4 elements per shortest wavelength, at the highest frequency of interest, insure convergence at high frequencies and accurate predictions for the entire observed frequency range [27]. Element densities between two and four elements per wavelength capture the response of the system correctly but lead to an slight overestimation of panel kinetic energy and radiated sound power at the upper end of the observed frequency range. Table 3.2 summarizes the frequency range, element distribution and applied criteria used in the prediction models.

Table 3.2: Frequency range and element grid definition.

Excitation	Frequency range	No. of elements x	y	Total No. of elements	Criterion x	y
APW	20 kHz	57	51	2907	$\Delta_x \leq \lambda_0/3.5$	$\Delta_y \leq \lambda_0/3.5$
ADF	12 kHz	39	35	1365	$\Delta_x \leq \lambda_0/4$	$\Delta_y \leq \lambda_0/4$
TBL	12 kHz	35	77	2695	$\Delta_x \leq \lambda_0/3.5$	$\Delta_y \leq \lambda_{conv.}/3.5$

Chapter 4

Structural response and sound radiation

At first the structural response and sound radiation of the aluminium panel and the composite sandwich panel due to deterministic and stochastic disturbances without active control are investigated. Significant differences in the panel response and sound radiation are observed for different types of disturbances. In the case of acoustic plane wave excitation a good agreement between the predicted numerical results and asymptotic analytic formula [3] are observed. Since radiation losses and fluid loading effects have been neglected, the spectrum of panel kinetic energy only depends on the characteristics of the disturbance and the panel structural response. The spectra of the radiated sound power also includes the radiation characteristics of the panels.

4.1 Dispersion curves and coincidence frequencies

Figure 4.1 shows the positive propagating bending wavenumber as a function of frequency for (a) the aluminium panel and (b) the composite sandwich panel. The circles represent the modal wavenumber components along the x- and y-axis. The wavenumber components satisfy the relationship $k_n = \sqrt{k_{x,n}^2 + k_{y,n}^2}$. The convective and acoustic wavenumber are given by the $k_{conv.} = \omega / U_{conv.}$ and $k_0 = \omega / c_0$ respectively. The frequency at which the bending wavenumber on the panel equals the acoustic wavenumber in air is

known as critical coincidence frequency. Potentially all resonant modes with wavenumber components close to the acoustic wavenumber are efficiently excited by an acoustic field. A convective coincidence occurs when the bending wavenumber in the direction of the flow on the panel equals the convective wavenumber of the turbulent boundary layer. Resonant modes with modal wavenumber components in stream wise y-direction ($white\ circles$) that are close to the convection wavenumber may be efficiently excited by the surface pressure fluctuation generated by the TBL.

At frequencies below 11 kHz the transverse wavenumber of the composite sandwich panel, shown in Figure 4.1(b), is lower than that for the aluminium panel, shown in Figure 4.1(a). The bending wavenumber for a given frequency is proportional to $\sqrt[4]{m''/D}$. Both panels have equal static stiffness but the aluminium panel has a four times higher mass per unit area. Thus, at low frequencies the bending wavenumber for the aluminium panel is $\sqrt{2}$ higher than those for the composite sandwich panel. The bending stiffness and modal density of the thin aluminium panel is constant with frequency. The equivalent bending stiffness of the sandwich panel is constant at low frequencies where it is determined by the bending stiffness of the cross-section. With increasing frequency the transverse shear distortion of the core layer causes a reduction of the equivalent bending stiffness which results in an increase in the modal density. At very high frequencies the bending wavenumber is determined by the faceplate bending stiffness and converges to a constant value, which is much higher than that of the thin homogeneous aluminium panel. In summary, at about 11 kHz both panel models produce similar bending wavelength and equal total mode count. Below 11 kHz the modal density of the aluminium panel is higher than that of the composite sandwich panel while above 11 kHz the modal density of the composite sandwich panel greatly exceeds that of the aluminium panel.

The lower wavenumbers on the composite sandwich panel at low frequencies result in lower coincidence frequencies than for the aluminium panel. For the aluminium panel the acoustic coincidence occurs at about 7.5 kHz. For the composite sandwich panel acoustic coincidence occurs at about 5.5 kHz. Efficient radiation modes that resonate around coincidence produce high structural response and sound radiation effects. Thus, according to the wavenumber plots in Figure 4.1, the composite sandwich panel is likely to radiate sound more efficiently than the aluminium panel for a wider range of audio frequencies.

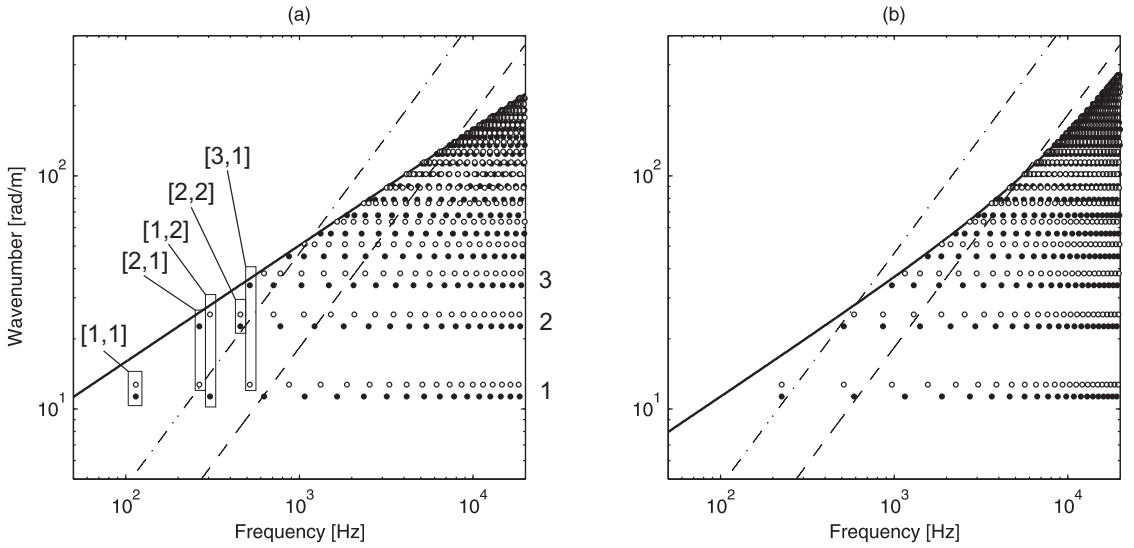

Figure 4.1: Propagating transverse wavenumber ($solid$) of the (a) aluminium and (b) composite sandwich panel; acoustic wavenumber ($dashed$) and convective wavenumber ($dash-dotted$). Wavenumber components of structural modes in span-wise x-direction ($black\,circles$) and in stream-wise y-direction ($white\,circles$).

For thin aluminium panels, the effect of acoustic coincidence often is not a problem for practical engineering applications since it occurs at the upper end of the audio frequency range where the structural response has already rolled off due to the mass effect and to effective passive treatments. For lightweight sandwich structures the coincidence frequency potentially occurs in the mid audio frequency range where the response of the panel is still controlled by clusters of modes. This might cause an undesired increase in sound radiation, since at low and mid audio frequencies the structural response of the the panel is not rolled off by the mass effect and passive control measures may not work effectively.

The convective coincidence frequency for the aluminium panel occurs at 1169 Hz and at 609 Hz for the composite sandwich panel. Due to the low coincidence frequency and low modal density, only a few structural modes of the composite sandwich panel resonate in the vicinity of the convective coincidence frequency. This indicates a potential for active structural control which tends to be particularly effective at controlling low frequency resonances. The effect of the convective coincidence is discussed in more detail in a later section of this report. The coincidence frequencies for the two panels are summarised in Table 4.1.

Table 4.1: Coincidence frequencies.

Panel	Acoustic critical frequency [Hz]	Excitation coincidence frequency [Hz] for APW θ=45°	Convective coincidence frequency [Hz] for TBL disturbance
Aluminium	7,544	15,087	1,169
Sandwich	5,489	190,663	609

4.2 Acoustic plane wave

Figure 4.2 shows the frequency spectrum of panel kinetic energy (left hand side column) and radiated sound power (right hand side column) of the aluminium panel ($solid\,line$) and composite sandwich panel ($faint\,line$) for a plane wave excitation. Three different angles of incidence are considered. These angles are θ = 0° (normal incidence), θ = 45° and θ = 90° (grazing incidence). The excitation angle $\varphi = 45°$ for all cases.

APW with θ = 0° (normal incidence): Figure 4.2(a) and (b) show the structural response and radiated sound power for both panels due to a plane wave excitation at normal incidence. Even structural modes are not excited. This is because the excitation field is uniform over the surface of the panel. Odd modes however are efficiently excited. Since the plane wave is incident normal to the panel surface no excitation coincidence effects are present in the kinetic energy and radiated sound power spectra. Above the first few resonances of the panel, the kinetic energy follows the mass law [3] and rolls off at a rate of 6 dB per octave, i.e. 20 dB per decade. In this mass controlled frequency band the panel kinetic energy of the composite sandwich panel is about 6 dB higher than that of the aluminium panel. This is because the aluminium panel has a four times higher mass per unit area. Corresponding low order resonant modes for both panels have a similar response magnitude.

The radiated sound power for both panels is the same at frequencies well below the first panel resonance. This is because the radiated sound power in this frequency band is determined by static stiffness which is equal for both panels. Above the first panel resonance the radiated sound powers are mass controlled up to about the critical frequencies [3] of the two panels. In the mass controlled region, the radiated sound power of the composite sandwich panel is 12 dB higher than that of the four times more heavy aluminium

panel. The radiated sound power of the aluminium panel follows the mass law up to 5 kHz. Around the critical frequency at about 7.5 kHz the radiated sound power increases because of the acoustic coincidence effect in the radiation properties of the panel (The radiation efficiencies of all modes peak at around the critical frequency [3]). The radiated sound power of the composite sandwich panel follows the mass law only up to 2 kHz. Around the critical frequency at bout 5.5 kHz the the radiated sound power increases because of the radiation acoustic coincidence effect. Around 5.5 kHz the radiated sound power spectra of the composite sandwich panel is more than 20 dB higher than that of the aluminium panel.

The radiation acoustic coincidence frequency range for the composite sandwich panel is wider than that for the thin homogeneous aluminium panel. This is due to the transition from bending to shear response which produces acoustic coincidence conditions over an extended frequency band. This effect can be visualised in the wavenumber plots of Figure 4.1. The lines for the acoustic wavenumber and the flexural wavenumber for the aluminium panel intersect at a rather wide angle at the critical frequency. In contrast the acoustic wavenumber and the transverse wavenumber lines for the composite sandwich panel intersect at a more narrow angle and remain quite close to each other above the critical frequency so that the radiation acoustic coincidence effect extends over a wider frequency band.

However, this radiation characteristic is not necessarily the same for all sandwich panels. In the shear-controlled transition region the transverse wavenumber for a sandwich panel tends to $k = k_s$ [3] where according to Equation (2.12) $k_s = \omega\sqrt{m''/Gd}$. If k_s is similar to the acoustic wavenumber $k_0 = \omega/c_0$ then the radiation acoustic coincidence frequency band is extremely wide. If however k_s is much higher than k_0 radiation coincidence should not occur until very high frequencies where the structural wavenumber is dominated by faceplate bending. Also if k_s is very low then radiation coincidence occurs at relatively low frequencies where the structural wavenumber is dominated by the bending of the overall sandwich cross-section. Thus the specific design of lightweight sandwich panels can significantly influence the radiation characteristics.

It is also interesting to note that at low frequencies the spectra of the radiated sound power of the aluminium panel are characterised by resonance and anti-resonance effects. This

occurs in between two resonances of structural modes that interfere destructively, causing a cancellation of the modal contributions to the radiated sound power.

APW with θ = 45°: Figure 4.2(c) and (d) show the panel response and radiated sound power for a plane wave incident at an angle θ = 45°. In this case all structural modes are efficiently excited. Above the first resonance, the structural response of the aluminium panel follows the mass law up to about 10 kHz. Around this frequency the spectrum of the panel kinetic energy shows a wide frequency band crest composed by a series of resonance peaks. This is because the projection of the acoustic excitation wave onto the panel surface for an angle θ = 45° is $\sqrt{2}$ longer than the acoustic wavelength. Thus, since the bending wavenumber is proportional to $\sqrt{f}$ an excitation coincidence effect occurs at twice the critical frequency, that is about 15 kHz. Around this coincidence frequency the response of the panel is dominated by resonances of discrete, efficiently excited modes whose responses are controlled by structural damping. Above this coincidence frequency the panel response is stiffness and mass controlled and rolls off rapidly at a rate of 36 dB per octave.

The structural response of the composite sandwich panel does not exhibit this excitation coincidence effect, which occurs at 190 kHz and is therefore outside the observed frequency range. This is because the structural wavenumber of the sandwich panel in the shear transition region is higher than the projected wavenumber of the acoustic excitation $\omega/(\sqrt{2}c_0)$. The response of the composite sandwich panel at high frequencies exhibits mass-controlled behaviour. However the roll off rate is lower than 6 dB per octave.

The radiated sound power of the aluminium panel is mass controlled up to 5 kHz. Above 5 kHz the radiated sound power spectra of the aluminium panel shows the combined effect of the radiation acoustic coincidence around the critical frequency at 7.5 kHz, and the excitation coincidence at 15 kHz. The radiated sound power spectra of the composite sandwich panel exhibits these radiation and excitation acoustic coincidence effects in the frequency range between 2 kHz and 10 kHz. At 5.5 kHz the radiated sound power of the composite sandwich panel is about 25 dB higher than that of the aluminium panel.

In comparison to the kinetic energy spectra, below the critical frequency some resonant peaks are significantly reduced in the spectrum of the radiated sound power. This is

because the surface pressure fluctuations caused by even modes counteract each other and are not efficiently radiated into the far field [3].

APW with θ = 90°: Figure 4.2(e) and (f) show the panel response and radiated sound power for a plane wave incident at an angle θ = 90° (grazing incidence). At this angle the plane wave excites all structural modes. For grazing incidence both, the excitation acoustic coincidence and the radiation acoustic coincidence occur at the critical frequency. This is because the wavelength of the acoustic excitation projects directly onto the panel surface. The response of the panels around critical frequency is dominated by discrete efficiently excited modes whose responses are controlled by structural damping. Above critical frequency the panel response is stiffness and mass controlled and rolls off rapidly. The response of the aluminium panel rolls off at a rate off 36 dB per octave. The response of the composite sandwich panel rolls off at a lower rate of about 16 dB per octave. This difference is caused by the shear distortion in the transverse wavenumber of the sandwich panel which results in a decrease in bending stiffness and thus results in an increase in modal density.

The spectra of the radiated sound power for frequencies up to 1 kHz are very similar to those for the plane wave incident at θ = 45°. For higher frequencies both panels show the overlaying acoustic coincidence effect in the excitation and the radiation characteristics. Around critical frequency the sound power spectra is dominated by individual efficiently radiating resonant modes. Above coincidence the radiated sound power of both panels rolls off rapidly with frequency. Around the acoustic critical frequency of the composite sandwich panel at 5.5 kHz the radiated sound power of the sandwich panel exceeds that of the aluminium panel by about 30 dB. Also in this case, below critical frequencies the amplitude of the resonance peak of even modes are rather small because of their low radiation efficiency.

4.3 Stochastic disturbances

Figure 4.3 shows the predicted panel kinetic energy (left hand side column) and radiated sound power (right hand side column) of the aluminium panel ($solid\,line$) and composite

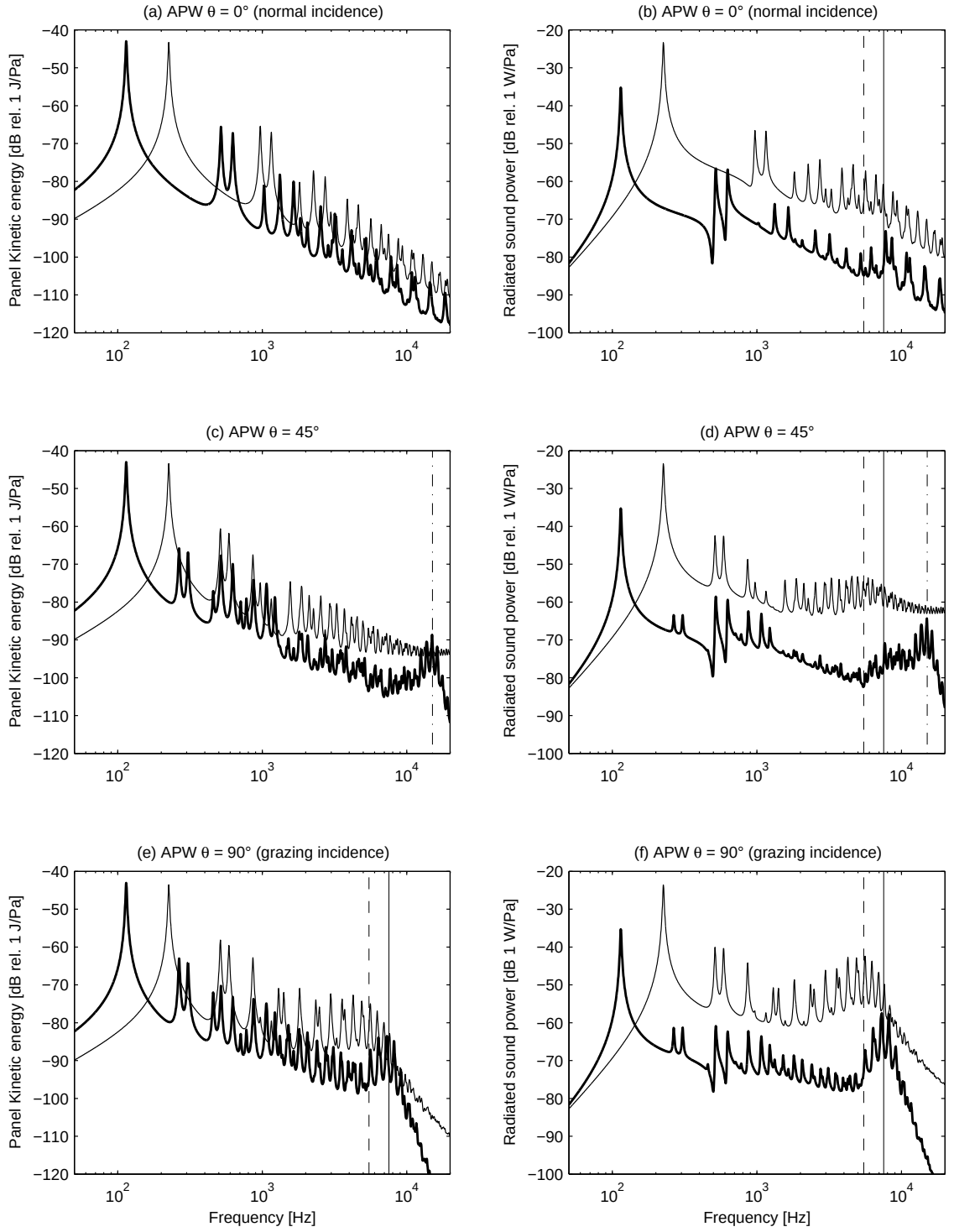

Figure 4.2: Panel kinetic energy and radiated sound power of the 1.6 mm aluminium panel ($solid$) and the composite sandwich panel with equivalent static bending stiffness ($faint$) for a acoustic plane wave incident at θ = 0°, 45° and 90°. Vertical lines mark the acoustical critical frequency of the aluminium panel ($solid$), composite sandwich panel ($dashed$) and the θ = 45° excitation coincidence frequency for the aluminium panel ($dash - dotted$).

sandwich panel ($faint\,line$) for acoustic diffuse field (top row) and turbulent boundary layer (bottom row) disturbances. The spectra are normalised to the power spectral densities of equivalent acoustic plane wave with a pressure amplitude of 1 Pa at all frequencies.

4.3.1 Acoustic diffuse field

Figure 4.3(a) and (b) show the structural response and radiated sound power of the aluminium panel and the composite sandwich panel for an acoustic diffuse field disturbance. As a comparison with Figure 4.2(c) and (d) shows, the low frequency structural response and radiated sound power of both panels up to 1 kHz is very similar to the response to an acoustic plane wave with incidence angles θ = 45° and φ = 45°.

Figure 4.3(a) shows that, at higher frequencies the structural response of the aluminium and composite sandwich panel are characterised by the excitation coincidence effect, which, for diffuse acoustic excitation, formed by acoustic waves at arbitrary random angles of incidence, occurs around the critical frequencies at 7.5 kHz and 5.5 kHz respectively. The panel response in coincidence region is characterised by resonating modes, but the response of individual modes is less pronounced than for the cases of APW excitation shown in Figure 4.2. Above the coincidence region the kinetic energy spectrum of both panels rolls off at a lower rate than for the cases of APW excitation. These differences in the response spectra can also be explained by the fact that the ADF excitation is formed by acoustic waves at arbitrary random angles of incidence. Figure 4.3(b) shows the spectrum of the radiated sound power of the panels for an acoustic diffuse field disturbance. As for the Acoustic plane wave excitation at grazing angle in Figure 4.2(e), the spectrum of radiated sound power in Figure 4.3(b) shows the combined effect of acoustic excitation coincidence and radiation coincidence, which cause a considerable increase of radiated sound power around the acoustic critical frequency.

4.3.2 Turbulent boundary layer

Figure 4.3(c) and (d) show the structural response and radiated sound power of both panels for the TBL disturbance. In the frequency range below 2 kHz the response of both panels is dominated by resonances of low order modes. For the aluminium panel the convective

coincidence occurs at 1169 Hz, while for the composite sandwich panel it occurs at 609 Hz. The panel response therefore depends on how efficiently specific modes are excited by the TBL disturbance. Above the convective coincidence region, the response of the aluminium panel drops off at a rate of 9 dB per octave. The roll off rate for the composite sandwich panel is slightly lower. This is due to the increase in modal density above 2 kHz.

The discussion on the response of low order structural modes to TBL disturbance requires to recall the properties of the correlation function for the TBL disturbance in Equation (3.17). Since the correlation function for the TBL in x-direction (span wise) is characterised by a monotonically decaying exponential function, there are no coincidence effects along the x-axis of the panels. Therefore only structural modes with modal wavenumber component in y-direction which is close to the convective wavenumber are characterised by a coincidence effect.

Table 4.2 gives the panel modes that are efficiently excited by coincidence with the TBL downstream convective field. Bold mode orders indicate efficiently radiating modes, modes in brackets indicate a group of modes that can not be distinguished as individual resonance peaks in Figure 4.3(c) and (d) and the dashed horizontal lines mark the convective coincidence frequency. The comparison between the two panels shows that, for the aluminium panel more modes are efficiently excited by the TBL disturbance than for the composite sandwich panel. A comparison of the results in Table 4.2 with Figure 4.1 shows that efficiently excited modes indeed have a wavenumber component in y-direction (stream wise) that is close to the convective wavenumber.

Table 4.2: Modes efficiently excited by TBL.

Aluminium panel			Composite sandwich panel		
Mode number	Frequency [Hz]	mode order (n_x, n_y)	Mode number	frequency [Hz]	mode order (n_x, n_y)
1	114	**(1,1)**	1	225	**(1,1)**
2	266	(2,1)	3	588	**(1,2)**
3	306	(1,2)	- - - - - - -	609	- - - - - - -
4	457	(2,2)	4	862	(2,2)
6	626	**(1,3)**	6	1155	**(1,3)**
7	710	(3,2)			
8	777	(2,3)			
10	1029	**(3,3)**			
11	1063	(4,2)			
12	1073	(1,4)			
- - - - - - -	1169	- - - - - - -			
13	1224	**(2,4)**			
16	1477	(3,4)			
18	1648	**(1,5)**			
19	1800	(2,5)			
26	2351	(1,6)			

The radiated sound power spectrum in Figure 4.3(d) shows that odd order modes in Table 4.2 radiate sound efficiently. Although even modes generally have a low radiation efficiently, the even [2,4] mode of the aluminium panel and the [1,2] mode of the composite sandwich panel also show high resonant peaks in the radiated sound power spectra in Figure 4.3(d). Comparison with Figure 4.1 shows that both modes have a wavenumber component in x-direction which is close to the acoustic wavenumber, which results in a high radiation efficiency.

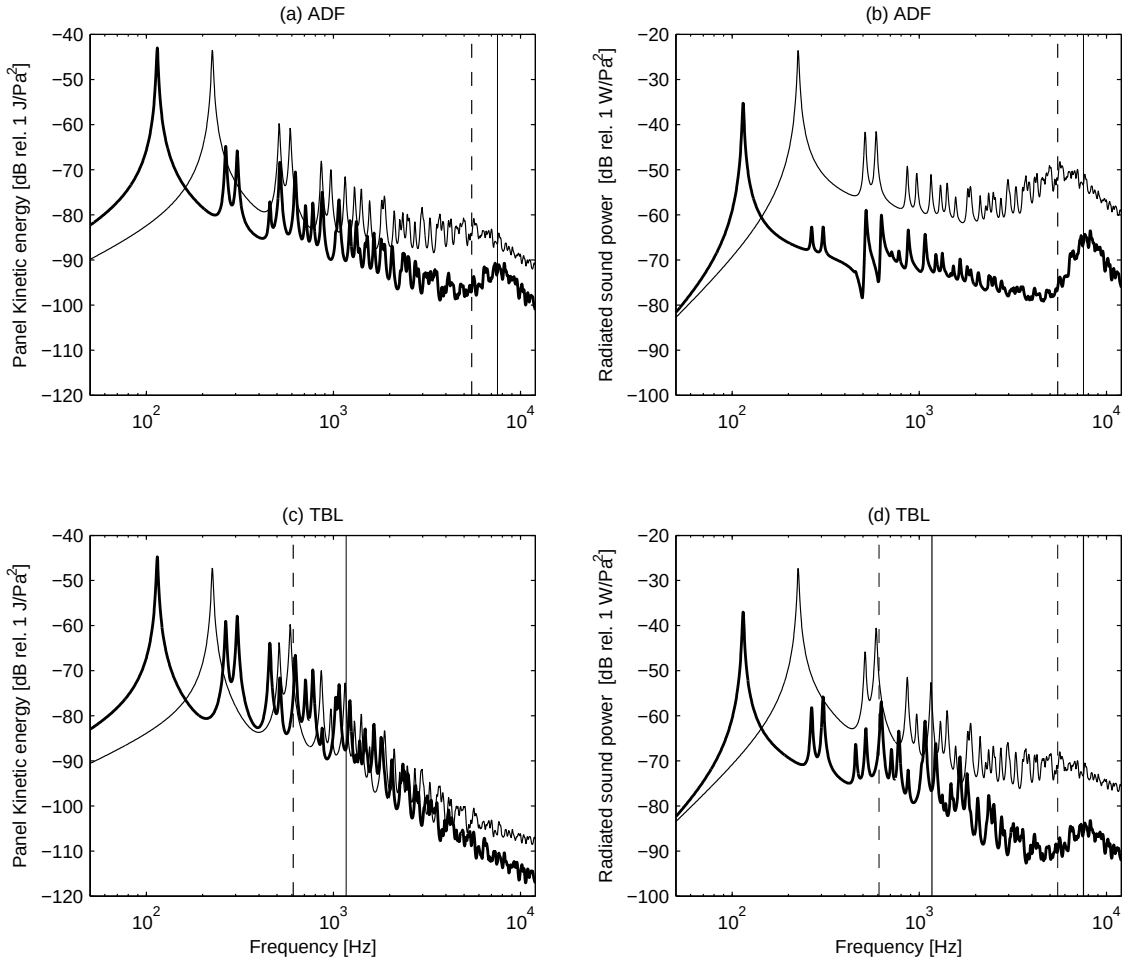

Figure 4.3: Panel kinetic energy and radiated sound power for the 1.6 mm Aluminium panel ($solid$) and the composite sandwich panel with equivalent static bending stiffness ($faint$) for ADF and TBL stochastic disturbances. Vertical lines mark the acoustical critical frequencies and aerodynamic coincidence frequencies of the aluminium panel ($solid$) and the composite sandwich panel ($dashed$).

Chapter 5

Decentralised velocity feedback control

In this section the structural response and sound radiation of the aluminium panel and the composite sandwich panel with active structural control for deterministic and stochastic disturbances are considered. As shown in Figure 2.1(b) and Figure 5.1, the panels are fitted with 16 decentralized ideal velocity feedback control loops. Figures 5.2 and 5.3 show the structural response and total radiated sound power for the aluminium panel (left hand side column) and the composite panel (right hand side column) with feedback gains in the range form 5 to 80. As discussed by Gardonio and Elliott [4], velocity feedback control introduces active damping. This allows to control the response of modes at resonance. At off resonance frequencies, active damping is not effective. For low feedback gains, the resonant peaks are initially damped and anti resonances in the radiated sound power spectra disappear. For increasing feedback gains new resonance behaviour starts to develop. For the composite sandwich panel this occurs for gains above 20 and for the aluminium panel for gains above 40. This difference relates to the structural impedances of the panels. Only with high feedback control gains the resonances of low order modes are completely cancelled by the sixteen feedback loops. In the high frequency region the control is limited by the large number of modes that contribute to the response at each frequency.

For all disturbances, the controllable frequency range for the composite sandwich panel extends to higher frequencies than for the aluminium panel. This is predominantly due to the lower modal density [3] on the composite sandwich panel but also to the lower convective and acoustic coincidence frequencies. At coincidence, the response of the

panels is dominated by the response of discrete resonant modes. These resonances can be effectively reduced by means of active velocity feedback. As shown in Figure 5.2 considerable reductions in the structural response of the aluminium panel can be achieved up to about 1.5 kHz for the APW (θ=45°), up to 2 kHz for the ADF and up to 3 kHz for TBL disturbance. For the composite sandwich panel considerable reductions of the response can be achieved for frequencies up to twice as high. As shown in Figure 5.3 considerable reductions in radiated sound power of the aluminium panel can be achieved up to 1 kHz for the APW (θ=45°) and ADF disturbances, while for the TBL disturbance considerable reductions are achieved up to 3 kHz. Also in this case, for the composite sandwich panel considerable reductions of the radiated sound power can be obtained for frequencies up to twice as high.

The predicted control performance for the structural response and radiated sound power for the TBL disturbance is much higher then those for Acoustic excitations. This is because the kinetic energy and radiated sound power spectra are dominated by a smaller number of resonant modes for which the k_y structural wavenumber coincides with the convective wavenumber of the TBL disturbance. The response and sound power radiation for APW and ADF disturbances is instead characterized by a large number of resonant modes, for which either the k_x or k_y structural wavenumbers components coincide with the acoustic wavenumber. Thus a large number of feedback control units would be required to obtain the same bandwidth as for the TBL excitation.

Figure 5.4 shows the spectrum of the radiated sound power of the aluminium panel excited by an ADF disturbance from Figure 5.3(c) on a linear frequency scale. The vertical line marks the acoustical critical frequency at 7.5 kHz. It is shown that, in the coincidence region around 7.5 kHz, with a feedback gain of 80 significant reductions of up to 7 dB can be achieved. This is because the panel response and radiated sound power around acoustic coincidence is dominated by the damping controlled response of discrete resonant modes. At these high frequencies, the bending wavelength on the panel is much shorter than the distance between the velocity sensor actuator pairs. One may therefore expect that the control performance for single modes will depend on the spatial distribution of the control units with respect to the shape of the modes. However, for stochastic disturbances a wide range of structural modes is excited at coincidence so that some reductions may be expected for even distributions of the control points. Reductions of the response and

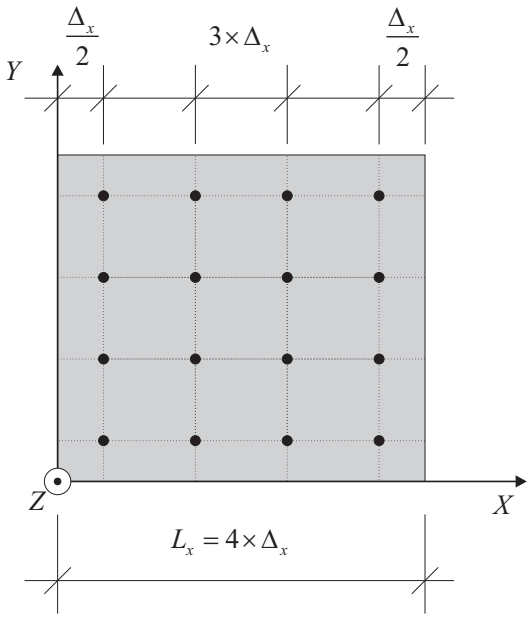

Figure 5.1: Spatial distribution of control loops across the panel.

radiated sound power in the coincidence region of thin aluminium panels might not be of practical interest because this effect occurs at the upper end of the audio frequency range and can be efficiently controlled by means of passive damping treatments. For composite sandwich panels the coincidence occurs at much lower frequencies and affects low order modes. In this case discrete velocity feedback is thought to be a promising and realisable control approach.

Figure 5.5 shows the achievable reduction in panel kinetic energy (left hand side column) and radiated sound power (right hand side column) for both panels for a feedback gain of 20 on a wavenumber scale. Normalising the spectra scale to the wavenumber corresponds to a normalisation of the stiffness to mass ratio of the two panels. The difference in the response is then given by the square root of the mass ratio. Since the aluminium panel is four times heavier than the composite panel, the control effort for similar reductions of the response of equal order modes is twice as high. For all disturbance cases the control reductions obtained for low order modes of the composite sandwich panel are significantly higher than those for corresponding modes of the aluminium panel. As show in Figure 5.5(b) and (d), for the acoustic disturbances considerably higher reductions in the radiated sound power of the composite sandwich panel are achieved for modes resonating around the acoustic coincidence wavenumber of the composite sandwich panel at 100 rad/m.

Figure 5.6 shows the 20 Hz to 12 kHz averaged reduction of the the A-weighted panel

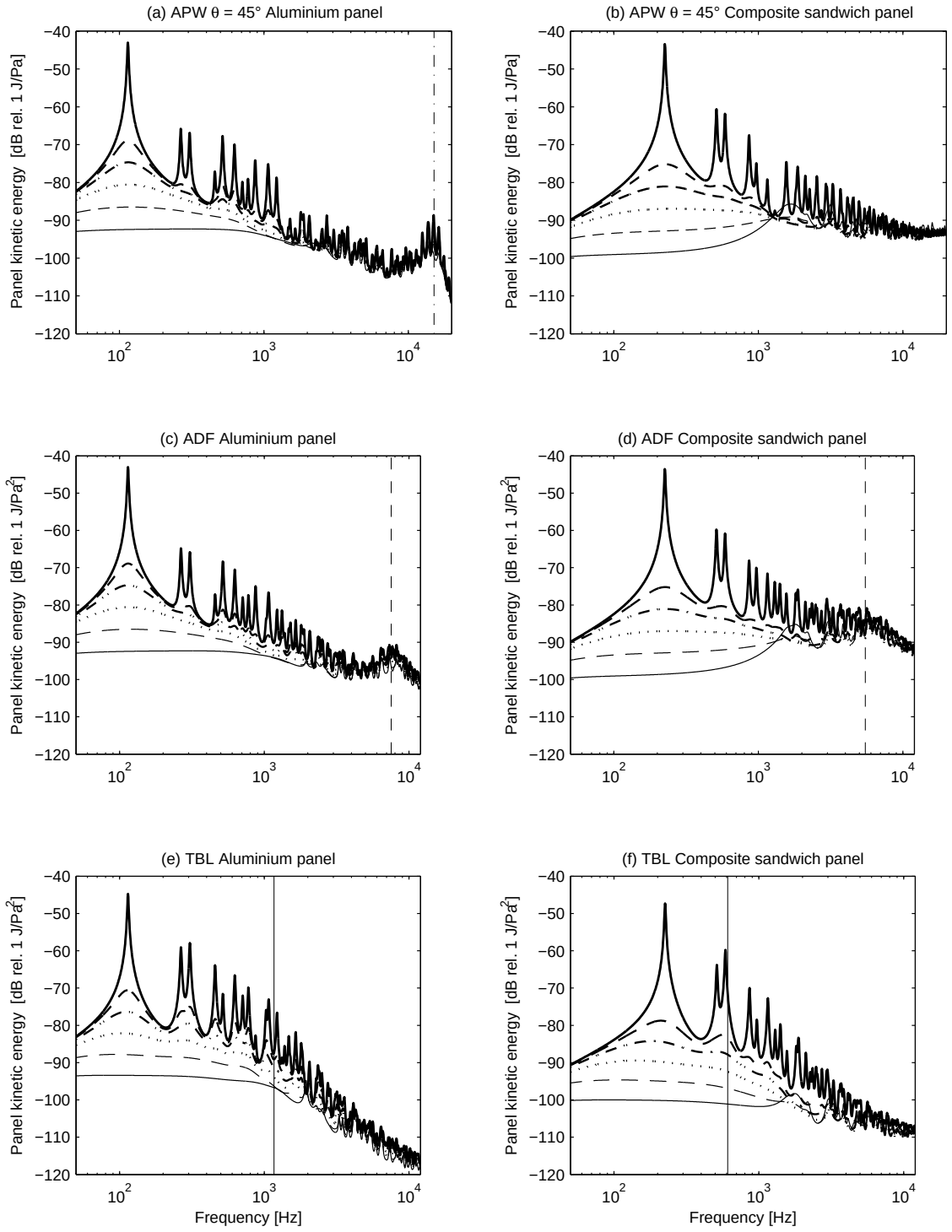

Figure 5.2: Kinetic energy of a 1.6 mm aluminium panel (left column) and a composite sandwich panel with equivalent static bending stiffness (right column) with 16 discrete idealized velocity feedback loops for APW (θ=45°) excitation and ADF and TBL stochastic disturbances. Passive panel ($solid$), feedback gain of 5 ($dashed$), 10 ($dash-dotted$), 20 ($dotted$), 40 ($faint$) and 80 ($faint-dashed$). Vertical lines mark the acoustical critical frequency ($dashed$) and convective coincidence frequency ($solid$).

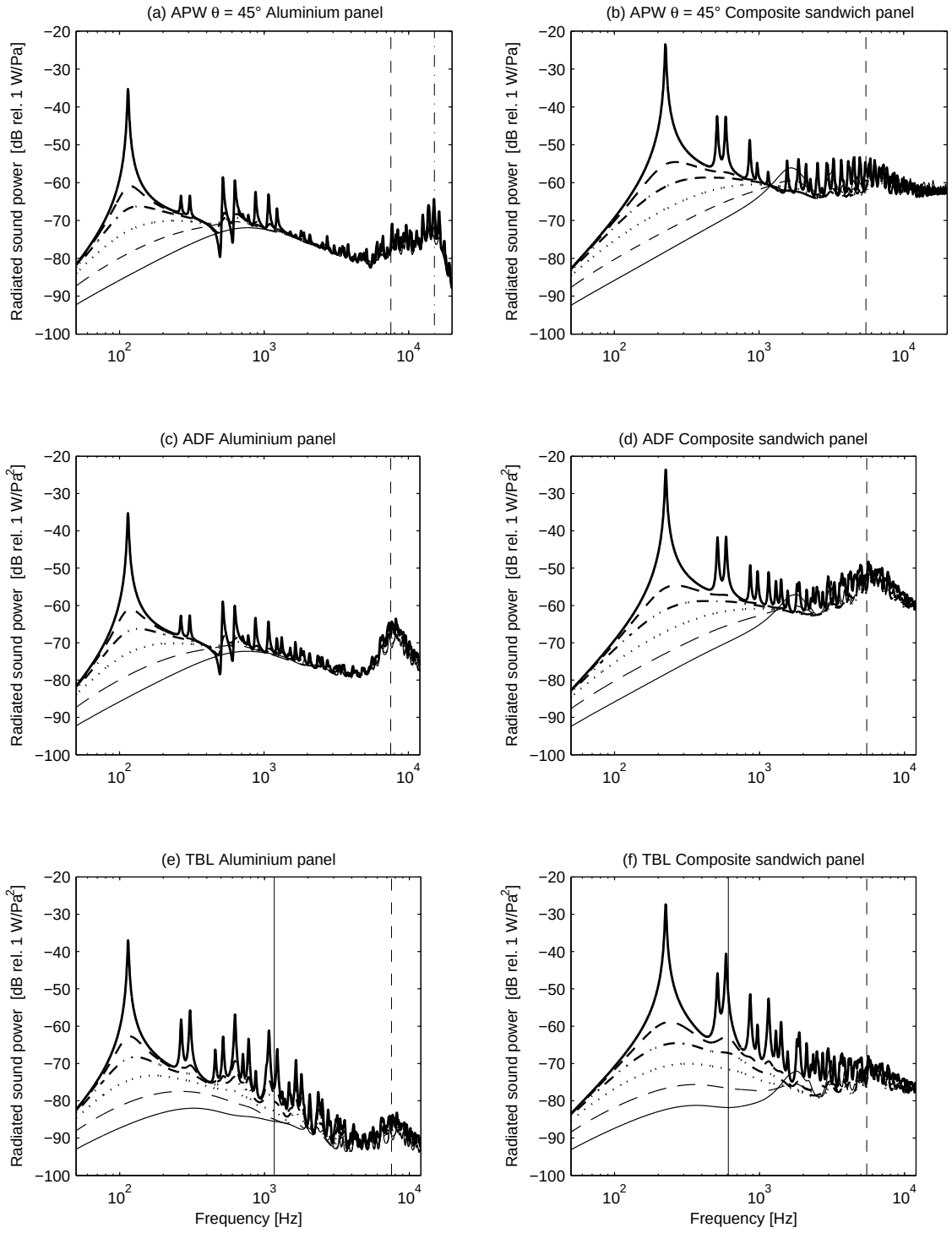

Figure 5.3: Radiated sound power from a 1.6 mm Aluminium panel (left column) and the composite sandwich panel with equivalent static bending stiffness (right column) with 16 discrete idealized velocity feedback loops for APW (θ=45°) excitation and ADF and TBL stochastic disturbances. Passive panel ($solid$), feedback gain of 5 ($dashed$), 10 ($dash-dotted$), 20 (dotted), 40 ($faint$) and 80 ($faint-dashed$). Vertical lines mark the acoustical critical frequency ($dashed$) and convective coincidence frequency ($solid$).

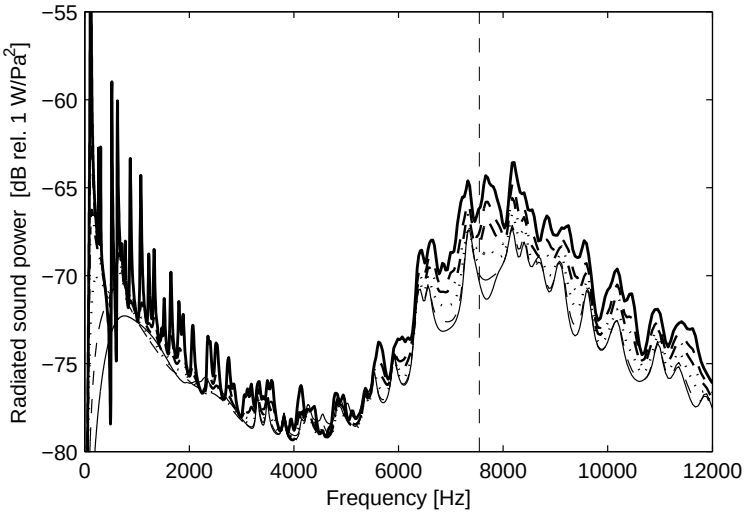

Figure 5.4: Radiated sound power from the 1.6 mm aluminium panel with 16 discrete idealized velocity feedback loops for a ADF disturbance and with a feedback gain of 5 ($dashed$), 10 ($dash - dotted$), 20 ($dotted$), 40 ($faint$) and 80 ($faint - dashed$). The vertical line marks the acoustical critical frequency ($dashed$).

kinetic energy (left hand side) and total sound power radiated (right hand side). This is thought to be a fair approach to assess the overall control performance of the two panels. The achieved reductions in the panel kinetic energy are generally higher then those for the radiated sound power. This is because the reductions in all resonant structural modes are reflected in the overall reductions in panel kinetic energy but only reductions in efficiently radiating modes affect the overall reduction in radiated sound power.

Considering the acoustic APW and ADF disturbance cases, for low feedback gains higher reductions are achieved for the smart composite sandwich panel than for the smart homogeneous aluminium panel. Optimal control performance for the composite sandwich panel is achieved for a feedback gain of 20. As shown in Figure 5.2 and Figure 5.3, for higher feedback gains new resonance behaviour starts to develop which diminishes the overall control performance. For higher feedback gains the predicted reductions for the aluminium panel are higher than those for the composite sandwich panel; for the kinetic energy this is for gains above 40 and for the radiated sound power this is for gains above 80. The highest reductions for the aluminium panel are achieved for a feedback gain of 80. The better control performance for the composite sandwich panel, in terms of reductions in A-weighted radiated sound power for a wide range of feedback gains is due to the control of the efficiently radiating modes in the mid audio frequency range.

In the case of the TBL excitation significant reductions in the structural response and

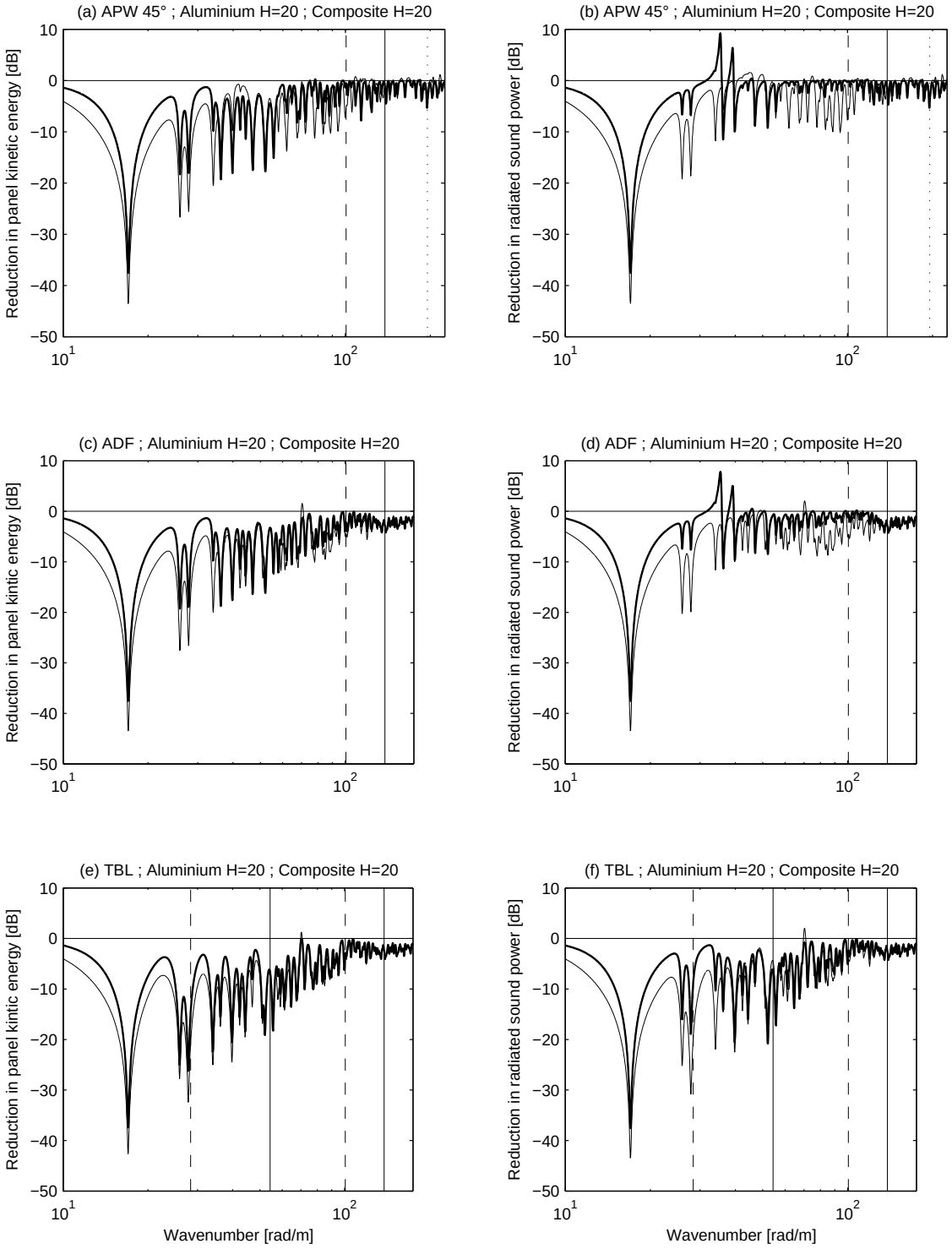

Figure 5.5: Reductions in panel kinetic energy and radiated sound power plotted over the structural wavenumber, for a 1.6 mm aluminium panel with **feedback gain of 20** ($solid$) and the composite sandwich panel with **feedback gain of 20** ($faint$) with 16 discrete idealized velocity feedback loops for APW (θ = 45°) ADF and TBL disturbance. Vertical lines mark the acoustical critical ($dashed$) and convective coincidence frequency ($solid$).

radiated sound power are predicted for both panels. This is because the TBL excitation excites predominantly low order structural modes whose wavenumber in in y-direction coincides with that of the stream wise convective field. These modes can be efficiently controlled by means of discrete velocity feedback. The high response of low order modes shifts the optimal control gain for both panels towards higher values. For low feedback gains the predicted reductions for the composite sandwich panel are up to 10 dB higher than those of the aluminium panel. This is partly because only a small number of low order structural modes of the composite sandwich panel are efficiently excited by the TBL (see Table 4.2), and because for equal feedback gains the response of low order structural modes of the composite sandwich panel are controlled more effectively than those of the aluminium panel (see Figure 5.5).

In practice it is difficult realise high feedback gains because control systems are often only conditionally stable and can also cause control spill over effects at low or high frequencies, depending on the type of actuator. The lower optimal feedback gain for the composite sandwich panel may therefore be beneficial for practical applications. Currently active control systems are mainly considered for low frequency noise applications up to 1 kHz. The results of this study indicate that it might be possible to extend the operative frequency range of active control systems up to mid audio frequencies when lightweight sandwich panels are used. In this case the benefits of active control systems could offset the additional costs and additional installed mass.

At mid frequencies at which the modal overlap is in the vicinity of unity, the response of the panels is mass controlled. Thus parts of the response can not be controlled by means of active damping. An ideal control system would therefore synthesise active damping at low frequencies where the response of the structure is controlled by well separated resonances of low order modes an distributed mass, i.e. distributed acceleration feedback, at higher frequencies where the modal overlap exceeds unity and therefore the response of the panel is controlled by the distributed mass of the partition.

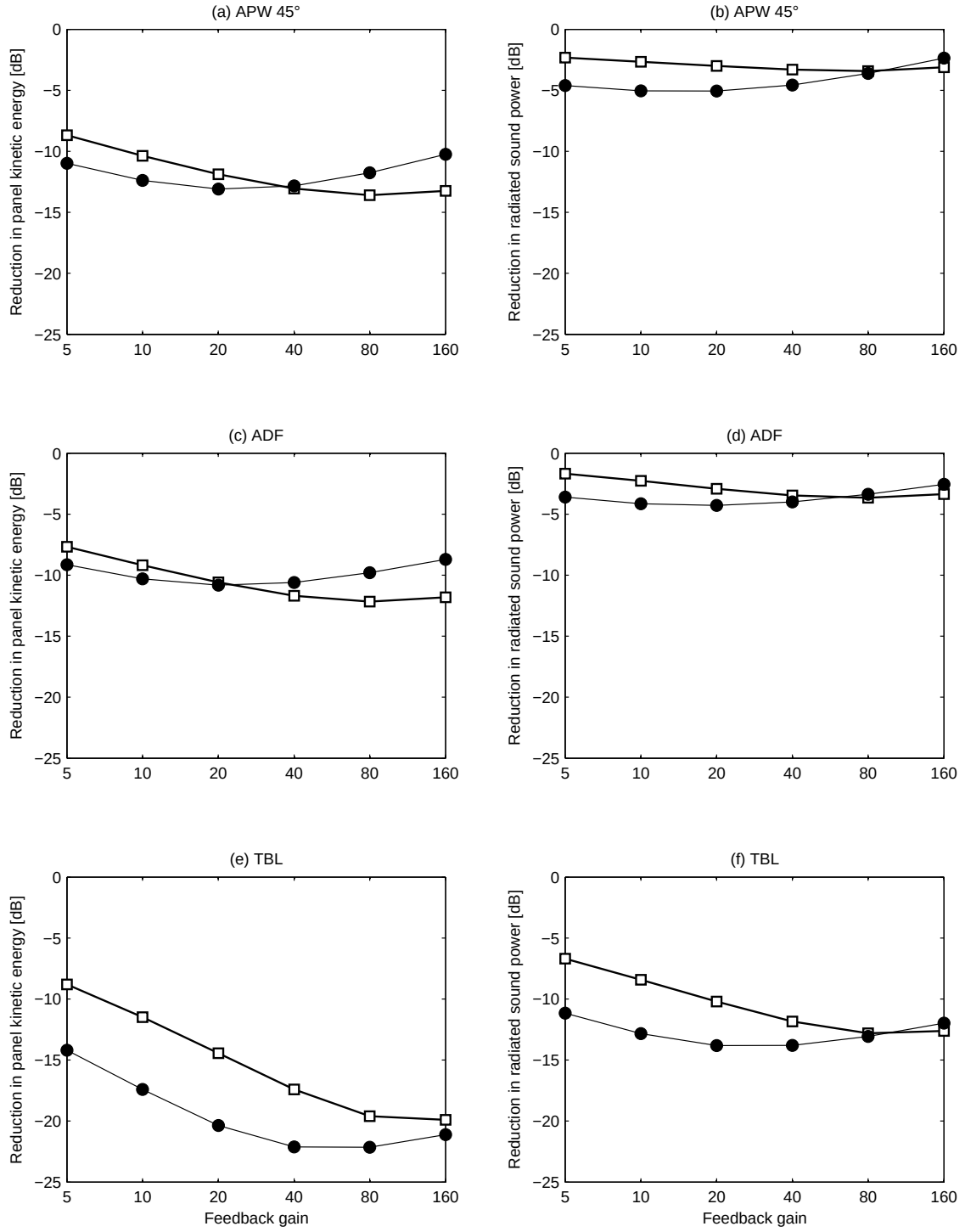

Figure 5.6: Overall reductions in A-weighted panel kinetic energy and radiated sound power for the panels with 16 discrete idealized velocity feedback loops. Aluminium panel ($solid\,line$ / $blanc\,sqares$), composite sandwich panel ($faint\,line$ / $black\,circles$) for a APW (θ = 45°), ADF and TBL disturbance.

Chapter 6

Conclusions

In this report two active panels under deterministic and stochastic excitation have been considered. The first panel is a homogeneous 1.6 mm thick aluminium while the second is a composite sandwich panel with equivalent static stiffness but four times lower mass per unit area. Firstly, the panels structural response and radiated sound power due to (a) acoustic plane wave, (b) stochastic acoustic diffuse field and (c) turbulent boundary layer disturbances have been investigated and contrasted. Secondly, the response of the panels with sixteen decentralised velocity feedback control loops using idealized point force actuators and collocated idealized velocity sensors was studied to compare the control effects on both panels and to investigate the intrinsic limits of decentralised velocity feedback control. In contrast to previous studies on active panels, the analysis has been extended to the upper end of the audio frequency range. Due to the low modal density and lower convective and acoustic coincidence frequency the response of the composite sandwich panel is dominated by discrete resonate modes over a wide range of audio frequencies. This indicates a high potential for the application of damping treatment to reduce the panel kinetic energy and radiated sound power. Passive treatments are not effective at low frequencies and might add high amount of mass which is diminishing the initial benefits of lightweight design. It has been demonstrated that for low feedback gains discrete active velocity feedback shows a better control performance for lightweight sandwich panel then for a homogeneous aluminium panel. This is particularly the case for TBL excitation where the structural response is dominated by low order resonant modes. Discrete velocity feedback is efficient in controlling the resonant response of low order

resonant modes and also in controlling the response of individual modes resonating at acoustic coincidence in the mid and high audio frequencies range.The results of this simulation study suggests that decentralised velocity feedback control is efficient in reducing the structural response and radiated sound power of a lightweight sandwich panel up to the mid and high audio frequencies. In this case the benefits of Active control systems could offset the additional costs and additional installed mass. In this report basic structural models and ideal velocity sensor actuator pairs have been considered. Further work is required to evaluate the control performance considering the dynamic response of the panels and actuator units in more detail.

Bibliography

[1] C. R. Fuller, S. J. Elliott and P. A. Nelson *Active Control of Vibration*. Academic Press, London, 1st edition, 1996.

[2] R. L. Clark, W. R. Saunders and G. P. Gibbs *Adaptive Structures, Dynamics and Control*. Wiley-Intersience, New York, NY, 1st edition, 1998.

[3] F. J. Fahy and P. Gardonio *Sound and Structural Vibration, radiation, transmission and resoponse*. Academic Press, Oxford, 2nd edition, 2007.

[4] P. Gardonio and S. J. Elliott Smart panels for active structural acoustic control. *Smart Materials and Structures*, 13(6):1314 – 36, 2004.

[5] C. R. Fuller Active control of sound transmission/radiation from elastic plates by vibration inputs. i. analysis. *Journal of Sound and Vibration*, 136(1):1 – 15, 1990.

[6] C. R. Fuller, C. H. Hansen and S. D. Snyder Active control of sound radiation from a vibrating rectangular panel by sound sources and vibration inputs. an experimental comparison. *Journal of Sound and Vibration*, 145(2):195 – 215, 1991.

[7] C. R. Fuller and R. A. Burdisso A wavenumber domain approach to the active control of structure-borne sound. *Journal of Sound and Vibration*, 148(2):355 – 60, 1991.

[8] C. R. Fuller, C. A. Rogers and H. H. Robertshaw Control of sound radiation with active/adaptive structures. *Journal of Sound and Vibration*, 157(1):19 – 39, 1992.

[9] C. R. Fuller and R. J. Silcox. Active structural acoustic control. *Journal of the Acoustical Society of America*, 91(1):519, 1992.

[10] B.-T. Wang, C. R. Fuller and E. K. Dimitriadis Active control of noise transmission through rectangular plates using multiple piezoelectric or point force actuators. *Journal of the Acoustical Society of America*, 90(5):2820–2830, 1991.

[11] R. L. Clark and C. R. Fuller. A model reference approach for implementing active structural acoustic control. *Journal of the Acoustical Society of America*, 92(3):1534 – 44, 1992.

[12] R. L. Clark and C. R. Fuller Experiments on active control of structurally radiated sound using multiple piezoceramic actuators. *Journal of the Acoustical Society of America*, 91(6):3313 – 20, 1992.

[13] R. L. Clark and C. R. Fuller. Active structural acoustic control with adaptive structures including wavenumber considerations. *Journal of Intelligent Material Systems and Structures*, 3(2):296 – 315, 1992.

[14] W. T. Baumann, W. R. Saunders and H. H. Robertshaw Active suppression of acoustic radiation from impulsively excited structures. *Journal of the Acoustical Society of America*, 90(6):3202 – 8, 1991.

[15] W. T. Baumann, F.-S. Ho and H. H. Robertshaw Active structural acoustic control of broadband disturbances. *Journal of the Acoustical Society of America*, 92(4):1998 – 2005, 1992.

[16] S. J. Elliott and M. E. Johnson. Radiation modes and the active control of sound power. *Journal of the Acoustical Society of America*, 94(4):2194 – 204, 1993.

[17] S. D. Snyder, N. Tanaka and Y. Kikushima The use of optimally shaped piezoelectric film sensors in the active control of free field structural radiation. part 1. feedforward control. *Transactions of the ASME. Journal of Vibration and Acoustics*, 117(3A):311 – 22, 1995.

[18] A. D. Pierce. *Acoustics: An introduction to its physical principles and applications*. Acoustical Society of America, Woodbury, New York, 1989.

[19] W. K. Blake. *Mechanics of flow-induced sound and vibration*, volume II of *Complex flow-structure interactions*. Academic press, Orlando, Florida, 1986.

[20] M. S. Howe. *Acoustics of fluid-structure interactions*. Cambridge University Press, Cambridge, 1998.

[21] D. J. Thompson and J. Dixon; edited by F. J. Fahy and J. G. Walker. *Vehicle Noise, Chapter 6 in Advanced Applications in Acoustics, Noise and Vibration*. Spon Press, London and New York, 2004.

[22] J. S. Mixson and J. S. Wilby edited by H. H. Hubbard *Aeroacoustics of Flight Vehicles, Theory and Practice, Chapter: Interior Noise*. NASA langley Research Center, Hampton, Virginia, 1995.

[23] G. Cousin. Sound from tbl induced vibrations, trita-fkt 1999:35. Technical report, Royal Institute of Technology KTH, Stockholm. Department of Vehicle Engineering, The Marcus Wallenberg Laboratory for Sound and Vibration Research MWL, 1999.

[24] M. E. Johnson and S. J. Elliott. Active control of sound radiation using volume velocity cancellation. *Journal of the Acoustical Society of America*, 98(4):2174 – 86, 1995.

[25] C. Maury, S. J. Elliott and P. Gardonio Turbulent boundary-layer simulation with an array of loudspeakers. *AIAA Journal*, 42(4):706 – 13, 2004.

[26] S. J. Elliott, P. Gardonio, T. C. Sors and M. J. Brennan. Active vibroacoustic control with multiple local feedback loops. *Journal of the Acoustical Society of America*, 111(2):908 – 15, 2002.

[27] J. Rohlfing and P. Gardonio. Active control of sound transmission through panels with flexible boundaries under detreministic and stochastic excitation. Technical report, University of Southampton, Institute of Sound and Vibration Research, ISVR Technical Memorandum No. 977, 2007.

[28] G. Kurtze and B. G. Watters. New wall design for high transmission loss or high damping. *Journal of the Acoustical Society of America*, 31(6):739–748, 1959.

[29] J. J. Tuma and R. A. Walsh. *Engeneering Mathematics Handbook*. McGraw-Hill, 4 edition, 1997.

[30] P. J. Shorter and R. S. Langley. On the reciprocity relationship between direct field radiation and diffuse reverberant loading. *Journal of the Acoustical Society of America*, 117(1):85 – 95, 2005.

[31] S. J. Elliott, C. Maury and P. Gardonio The synthesis of spatially correlated random pressure fields. *Journal of the Acoustical Society of America*, 117(3):1186 – 201, 2005.

[32] G. M. Corcos. The resolution of pressures in turbulence. *Journal of the Acoustical Society of America*, 35:192–199, 1963.

[33] S. H. Crandall and W. D. Mark. *Random Vibration in Mechanical Systems*. Academic Press Inc. New York and London, 1963.

[34] D. E. Newland. *Random vibrations, spectral and wavelet analysis*. Longman Singapore Publishers Pte Ltd, 1993.

[35] P. A. Nelson and S. J. Elliott. *Active Control of Sound*. Academic Press London and San Diego, 1993.

Appendix A

Formulations for kinetic energy and radiated sound power

In this appendix the formulations for a) the panel kinetic energy and radiated sound power due to harmonic deterministic excitations and b) the spectral density of panel kinetic energy and radiated sound power due to stochastic disturbances are presented.

A.1 Notations for the time harmonic response of the panel

At first the notation for the time harmonic excitation and vibration velocity response of a rectangular panel, as shown in Figure 2.1 are introduced. This notation is then used to derive the formulations for the panel structural response and sound radiation for time harmonic and stochastic disturbances. Assuming time harmonic behaviour, of the form $Re\{\exp(j\omega t)\}$, where ω is the angular frequency and $j = \sqrt{-1}$, the transverse force excitation and the transverse velocity response of a panel can be expressed as

$$f(x,y,t) = Re\left\{\tilde{f}(x,y,\omega)e^{j\omega t}\right\}, \tag{A.1}$$

$$\dot{w}(x,y,t) = Re\left\{\tilde{\dot{w}}(x,y,\omega)e^{j\omega t}\right\}, \tag{A.2}$$

where $\tilde{f}$ and $\tilde{\dot{w}}$ are frequency-dependent complex phasors of the excitation force per unit

area and the velocity response.

A.1.1 Modal formulation

The time-dependent velocity response, can be expressed in terms of the following infinite modal summation [3]

$$\dot{w}(x,y,t) = Re\left\{\sum_{r=1}^{\infty}\phi_r(x,y)\dot{a}_r(t)e^{j\omega t}\right\}, \tag{A.3}$$

where $\phi_r(x,y)$ is the r-th natural mode and $\tilde{\dot{a}}_r(\omega)$ is the complex modal velocity. Thus the complex frequency-dependent velocity response is given by

$$\tilde{\dot{w}}(x,y,\omega) = \sum_{r=1}^{\infty}\phi_r(x,y)\tilde{\dot{a}}_r(\omega). \tag{A.4}$$

The frequency-dependent complex modal velocities $\tilde{\dot{a}}_r(\omega)$ can be expressed as the product of a resonant term and a modal or generalised excitation term of the form

$$\tilde{\dot{a}}_r(\omega) = \tilde{\Omega}_r\,\tilde{F}_r(\omega). \tag{A.5}$$

Considering a hysteresis damping model, the resonant term is given by

$$\tilde{\Omega}_r = \frac{j\omega}{M_r\left[\omega_r^2(1+j\eta)-\omega^2\right]} \tag{A.6}$$

where ω_r is the r-th natural frequency, η is the modal damping loss factor and M_r is the modal mass for the r-th natural mode, which is given by

$$M_r = \rho h\int_0^{l_x}\int_0^{l_y}\left[\phi_r(x,y)\right]^2 dx\,dy, \tag{A.7}$$

where ρ is the panel mass density and h is the panel thickness. If the panel is simply supported, the mass-normalised natural modes $\phi_r(x,y)$ are given by

$$\phi_r(x,y) = 2\sin\left(\frac{m_r\pi x}{l_x}\right)\,\sin\left(\frac{n_r\pi y}{l_y}\right) \tag{A.8}$$

where, m_r is the modal order in x-direction and n_r is the modal order in y-direction for the r-th mode. In this case $M_r = \rho h\, l_x\, l_y = M$, where M is the total mass of the panel. The corresponding modal excitation term is given by

$$\tilde{F}_r(\omega) = \int_0^{l_x}\int_0^{l_y} \phi_r(x,y)\,\tilde{f}(x,y,\omega)\,dx\,dy, \tag{A.9}$$

where $\tilde{f}(x,y,\omega)$ is the exciation force per unit area.

Mode truncation

If the modal summation in Equation (A.4) is truncated to the sum over the first N modal terms, so that

$$\tilde{\dot{w}}(x,y,\omega) \approx \sum_{r=1}^{N} \phi_r(x,y)\tilde{\dot{a}}_r(\omega), \tag{A.10}$$

after substituting Equation (A.5), the velocity at an arbitrary point of the panel can be cast into the following matrix formulation

$$\tilde{\dot{w}}(x,y,\omega) = \mathbf{\Phi}\,\tilde{\dot{\mathbf{a}}} = \mathbf{\Phi}\,\tilde{\mathbf{\Omega}}\,\tilde{\mathbf{F}}, \tag{A.11}$$

where

$$\tilde{\mathbf{\Omega}} = \begin{bmatrix} \tilde{\Omega}_1 & & \\ & \ddots & \\ & & \tilde{\Omega}_N \end{bmatrix} \tag{A.12}$$

is a diagonal matrix with the first N resonant terms in Equation (A.6) and

$$\mathbf{\Phi} = \begin{bmatrix} \phi_1(x,y) & \phi_2(x,y) & \cdots & \phi_N(x,y) \end{bmatrix}, \tag{A.13}$$

$$\tilde{\dot{\mathbf{a}}} = \left[\begin{array}{cccc} \tilde{\dot{a}}_1 & \tilde{\dot{a}}_2 & \cdots & \tilde{\dot{a}}_N \end{array} \right]^T, \tag{A.14}$$

$$\tilde{\mathbf{F}} = \left[\begin{array}{cccc} \tilde{F}_1 & \tilde{F}_2 & \cdots & \tilde{F}_N \end{array} \right]^T, \tag{A.15}$$

are respectively a row vector with the first N natural modes, a column vector with the first N modal velocities and a column vector with the first N modal excitations. Note that the modal excitation terms in Equation (A.15) involves the derivation of the spatial integrals in Equation (A.9).

A.1.2 Elemental approach

In the elemental approach the panel surface is subdivided in a uniform grid of N_e elements. The excitation and response is defined at the element centres. This allows to replacing the integration over the panel dimensions in Equation (A.9) by a finite sum over element contributions to give

$$\tilde{F}_r(w) \approx \sum_{i=1}^{N_e} \phi_r(x_i, y_i)\, A_e\, \tilde{f}(x_i, y_i, \omega), \tag{A.16}$$

where $\phi_r(x_i, y_i)$ is the mass-normalised natural mode evaluated at the centre of element i, A_e is the area of a single element and $\tilde{f}(x_i, y_i, \omega)$ is the force per unit area at the centre of the element, so that the product $A_e\, \tilde{f}(x_i, y_i, \omega)$ approximates the total force over the element surface. The vector with the elemental velocities

$$\tilde{\dot{\mathbf{w}}}_e = \left[\begin{array}{cccc} \tilde{\dot{w}}_{e_1} & \tilde{\dot{w}}_{e_2} & \cdots & \tilde{\dot{w}}_{e_{N_e}} \end{array} \right]^T \tag{A.17}$$

can be derived from equation (A.11) as follows

$$\tilde{\dot{\mathbf{w}}}_e(\omega) = \mathbf{\Phi}_e \tilde{\dot{\mathbf{a}}} = \mathbf{\Phi}_e \tilde{\mathbf{\Omega}} \mathbf{\Phi}_e^T \tilde{\mathbf{F}}_e \tag{A.18}$$

where $\mathbf{\Phi}_e$ is a $[N_e \times N]$ dimensional matrix of N_e rows with the first N natural modes at

the the centres of the panel elements

$$\mathbf{\Phi}_e = \begin{bmatrix} \phi_1(x_1, y_1) & \cdots & \phi_N(x_1, y_1) \\ \vdots & \ddots & \vdots \\ \phi_1(x_{N_e}, y_{N_e}) & \cdots & \phi_N(x_{N_e}, y_{N_e}) \end{bmatrix} \tag{A.19}$$

and $\tilde{\mathbf{F}}_e$ is the N_e-dimensional vector of discrete eqivalent excitation forces at the centres of the panel elements

$$\tilde{\mathbf{F}}_e = \begin{bmatrix} \tilde{F}_{e_1} & \tilde{F}_{e_2} & \cdots & \tilde{F}_{e_{N_e}} \end{bmatrix}^T. \tag{A.20}$$

The approximation of the surface integrals in Equation (A.9) by the sum over element contributions allows to consider complex natural mode functions, due to arbitrary boundary conditions and arbitrary spatial excitation fields.

A.2 Time-averaged total panel kinetic energy

The instantaneous total kinetic energy of the panel is given by the product of the panel density per unit area and the squared panel velocity integrated over the panel surface [3]:

$$E(t) = \frac{1}{2} \int_0^{l_x} \int_0^{l_y} \rho h \, \dot{w}^2(x, y, t) dx \, dy, \tag{A.21}$$

where l_x and l_y are the dimensions of a rectangular panel, ρh is the panel mass per unit area and $\dot{w}(x, y, t)$ is the transverse panel velocity. Assuming the panel mass per unit area is constant, Equation (A.21) can be rewritten as

$$E(t) = \frac{\rho h}{2} \int_0^{l_x} \int_0^{l_y} \dot{w}^2(x, y, t) dx \, dy, \tag{A.22}$$

The time averaged total panel energy is given by [33, 34]:

$$\overline{E} = \frac{\rho h}{2} \int_0^{l_x} \int_0^{l_y} \frac{1}{T} \int_0^T \dot{w}^2(x,y,t) dt\, dx\, dy \tag{A.23}$$

where T is a suitable period of time over which the mean square velocity is estimated; e.g. for time harmonic vibration , T is the period. Assuming time harmonic vibration as given in Equation (A.2), the time average integral can be rewritten in terms of the magnitude of the complex panel velocity $\tilde{\dot{w}}(x,y,\omega)$ to give

$$\frac{1}{T} \int_0^T \dot{w}^2(x,y,t) dt = \frac{1}{2} \left| \tilde{\dot{w}}(x,y,\omega) \right|^2, \tag{A.24}$$

which yields the time averaged total kinetic energy of the panel as

$$\overline{E} = E(\omega) = \frac{\rho h}{4} \int_0^{l_x} \int_0^{l_y} \left| \tilde{\dot{w}}(x,y,\omega) \right|^2 dx\, dy. \tag{A.25}$$

A.2.1 Modal formulation

Using the vector notation for the truncated modal summation of the transverse velocity of the panel given in Section A.1.1, the total panel kinetic energy in Equation (A.25) can be rewritten as

$$\begin{aligned} E(\omega) &= \frac{\rho h}{4} \int_0^{l_x} \int_0^{l_y} \tilde{\dot{\mathbf{a}}}^H(\omega)\, \mathbf{\Phi}^T\, \mathbf{\Phi}\, \tilde{\dot{\mathbf{a}}}(\omega)\, dx\, dy, \\ &= \frac{\rho h}{4}\, \tilde{\dot{\mathbf{a}}}^H(\omega) \int_0^{l_x} \int_0^{l_y} \mathbf{\Phi}^T\, \mathbf{\Phi}\, dx\, dy\, \tilde{\dot{\mathbf{a}}}(\omega), \end{aligned} \tag{A.26}$$

where ^{H} denotes the hermitian transpose. Considering mass normalized modes, the orthogonality property gives

$$\int_0^{l_x}\int_0^{l_y} \phi_r(x,y)\,\phi_s(x,y)\,dx\,dy = 0 \tag{A.27}$$

and

$$\int_0^{l_x}\int_0^{l_y} \phi_r(x,y)\phi_r(x,y)dx\,dy = l_x l_y. \tag{A.28}$$

Thus the integration over the panel surface in Equation (A.26) results in

$$\begin{aligned} E(\omega) &= \frac{\rho h}{4}\begin{bmatrix} \tilde{\dot{a}}_1^* & \tilde{\dot{a}}_2^* & \cdots & \tilde{\dot{a}}_N^* \end{bmatrix}\begin{bmatrix} \int\int \phi_1\phi_1 & \cdots & \int\int \phi_1\phi_N \\ \vdots & \ddots & \vdots \\ \int\int \phi_N\phi_1 & \cdots & \int\int \phi_N\phi_N \end{bmatrix}\begin{bmatrix} \tilde{\dot{a}}_1 \\ \vdots \\ \tilde{\dot{a}}_N \end{bmatrix} \\ &= \frac{\rho h}{4}\begin{bmatrix} \tilde{\dot{a}}_1^* & \tilde{\dot{a}}_2^* & \cdots & \tilde{\dot{a}}_N^* \end{bmatrix}\begin{bmatrix} l_x l_y & & \\ & \ddots & \\ & & l_x l_y \end{bmatrix}\begin{bmatrix} \tilde{\dot{a}}_1 \\ \vdots \\ \tilde{\dot{a}}_N \end{bmatrix}, \end{aligned} \tag{A.29}$$

which can be expressed in terms of the modal velocities vector defined in Equation (A.14):

$$\begin{aligned} E(\omega) &= \frac{\rho h\, l_x l_y}{4}\begin{bmatrix} \tilde{\dot{a}}_1^* & \cdots & \tilde{\dot{a}}_N^* \end{bmatrix}\begin{bmatrix} \tilde{\dot{a}}_1 \\ \vdots \\ \tilde{\dot{a}}_N \end{bmatrix} \\ &= \frac{M}{4}\,\tilde{\dot{\mathbf{a}}}^H(\omega)\,\tilde{\dot{\mathbf{a}}}(\omega), \end{aligned} \tag{A.30}$$

where M represents the total mass of the panel.

A.2.2 Elemental approach

In the elemental approach the spatial integral in Equation (A.25) is replaced by a summation over a grid of elements to give

$$
\begin{aligned}
E(\omega) &= \frac{\rho h}{4} \sum_{i=1}^{N_e} A_e \, |\tilde{\dot{w}}(x_i, y_i, \omega)|^2 \\
&= \frac{M_e}{4} \sum_{i=1}^{N_e} |\tilde{\dot{w}}(x_i, y_i, \omega)|^2. \qquad \text{(A.31)}
\end{aligned}
$$

where A_e and M_e the area and mass of a single panel element. Using the matrix notation for the element approach in Section A.1.2 this can be written as

$$
\begin{aligned}
E(\omega) &= \frac{M_e}{4} \begin{bmatrix} \tilde{\dot{w}}_1^* & \cdots & \tilde{\dot{w}}_{N_e}^* \end{bmatrix} \begin{bmatrix} \tilde{\dot{w}}_1 \\ \vdots \\ \tilde{\dot{w}}_{N_e} \end{bmatrix} \\
&= \frac{M_e}{4} \, \tilde{\dot{\mathbf{w}}}_e^{\,H}(\omega) \, \tilde{\dot{\mathbf{w}}}_e(\omega). \qquad \text{(A.32)}
\end{aligned}
$$

A.3 Time-averaged total radiated sound power

The instantaneous total sound power radiated is given by the product of panel velocity and acoustic pressure on the panel surface, integrated over the dimensions of the panel [3]:

$$
P(t) = \int_0^{l_x} \int_0^{l_y} \dot{w}(x, y, t) \, p(x, y, 0, t) dx \, dy, \qquad \text{(A.33)}
$$

where $\dot{w}(x, y, t)$ is the panel velocity and $p(x, y, 0, t)$ is the surface sound pressure on the radiating side of the panel. The time-averaged total radiated sound power is given by [33, 34]

$$
\overline{P} = \int_0^{l_x} \int_0^{l_y} \frac{1}{T} \int_0^{T} \dot{w}(x, y, t) \, p(x, y, 0, t) \, dt \, dx \, dy \qquad \text{(A.34)}
$$

where T is a suitable period of time over which to estimate the mean radiated sound

power. Assuming time harmonic vibration the time average integral can be rewritten in terms of the complex panel velocity $\tilde{\dot{w}}(x, y, \omega)$ and complex surface pressure fluctuations $\tilde{p}(x, y, 0, \omega)$

$$\overline{P} = P(\omega) = \frac{1}{2} \int_0^{l_x} \int_0^{l_y} Re \left\{ \tilde{\dot{w}}^*(x, y, \omega)\, \tilde{p}(x, y, 0, \omega) \right\} dx\, dy. \tag{A.35}$$

The complex surface pressure $\tilde{p}(x, y, 0, \omega)$ for time harmonic vibrations of a planar surface is given by the Rayleigh integral [3]

$$\tilde{p}(x, y, 0, \omega) = \frac{j\omega\rho_0}{2\pi} \int_0^{l_x} \int_0^{l_y} \tilde{\dot{w}}(x', y', \omega)\, \frac{e^{-jk_0 R}}{R}\, dx'\, dy' \tag{A.36}$$

where $R = \sqrt{(x - x')^2 + (y - y')^2}$ is the distance between two points on the panel, k_0 is the acoustic wavenumber in the surrounding media and ρ_0 is the mass density of the surrounding media on the radiating side of the panel. Thus substituting Equation (A.36) into Equation (A.35) gives

$$\begin{aligned}
P(\omega) &= \frac{1}{2} Re \left\{ \int_0^{l_x} \int_0^{l_y} \tilde{\dot{w}}(x, y, \omega)^* \frac{j\omega\rho_0}{2\pi} \int_0^{l_x} \int_0^{l_y} \tilde{\dot{w}}(x', y', \omega)\, \frac{e^{-jk_0 R}}{R}\, dx\, dy\, dx'\, dy' \right\} \\
&= \frac{1}{2} Re \left\{ \int_0^{l_x} \int_0^{l_y} \int_0^{l_x} \int_0^{l_y} \frac{j\omega\rho_0}{2\pi} \left[\frac{\cos(kR) - j\sin(kR)}{R} \right] \tilde{\dot{w}}^*(x, y, \omega)\, \tilde{\dot{w}}(x', y', \omega)\, dx\, dy\, dx'\, dy' \right\} \\
&= \frac{\omega\rho_0}{4\pi} \int_0^{l_x} \int_0^{l_y} \int_0^{l_x} \int_0^{l_y} \frac{\sin(kR)}{R}\, \tilde{\dot{w}}^*(x, y, \omega)\, \tilde{\dot{w}}(x', y', \omega)\, dx\, dy\, dx'\, dy' \\
&= \frac{\omega^2\rho_0}{4\pi c_0} \int_0^{l_x} \int_0^{l_y} \int_0^{l_x} \int_0^{l_y} \frac{\sin(kR)}{kR}\, \tilde{\dot{w}}^*(x, y, \omega)\, \tilde{\dot{w}}(x', y', \omega)\, dx\, dy\, dx'\, dy',
\end{aligned} \tag{A.37}$$

where * is the complex conjugate operator.

A.3.1 Modal formulation

Substituting the modal expression for the transverse velocity of Equation (A.4) into Equation (A.37) gives

$$\begin{aligned} P(\omega) &= \frac{\omega^2\rho_0}{4\pi c_0}\int_0^{l_x}\int_0^{l_y}\int_0^{l_x}\int_0^{l_y}\frac{\sin(kR)}{kR}\sum_{r=1}\phi_r(x,y)\tilde{\dot{a}}_r^*\sum_{s=1}\phi_s(x',y')\tilde{\dot{a}}_s\,dx\,dy\,dx'\,dy' \\ &= \sum_{r=1}\sum_{s=1}\tilde{\dot{a}}_r^*\tilde{\dot{a}}_s\frac{\omega^2\rho_0}{4\pi c_0}\int_0^{l_x}\int_0^{l_y}\int_0^{l_x}\int_0^{l_y}\phi_r(x,y)\frac{\sin(kR)}{kR}\,\phi_s(x',y')dx\,dy\,dx'\,dy' \end{aligned} \quad \text{(A.38)}$$

Considering the vector notation for modal truncation to the first N terms in Section A.1.1, Equation (A.38) can be casted in the the following matrix formulation [3]

$$\begin{aligned} P(\omega) &= \left[\begin{array}{ccc}\tilde{\dot{a}}_1^*\cdots & \tilde{\dot{a}}_N^*\end{array}\right]\left[\begin{array}{ccc}A_{1,1} & \cdots & A_{1,N}\\ \vdots & \ddots & \vdots\\ A_{N,1} & \cdots & A_{N,N}\end{array}\right]\left[\begin{array}{c}\tilde{\dot{a}}_1\\ \cdots\\ \tilde{\dot{a}}_N\end{array}\right] \\ &= \tilde{\dot{\mathbf{a}}}^H\,\mathbf{A}\,\tilde{\dot{\mathbf{a}}}, \end{aligned} \quad \text{(A.39)}$$

where $\mathbf{A}$ is the power transfer matrix with the elements $A_{r,s}$ given by

$$A_{r,s} = \frac{\omega\rho_0}{4\pi}\int_0^{l_x}\int_0^{l_y}\int_0^{l_x}\int_0^{l_y}\phi_r(x,y)\,\frac{\sin\left(k_0R\right)}{R}\,\phi_s(x',y')\,dx\,dy\,dx'\,dy'. \quad \text{(A.40)}$$

A.3.2 Elemental approach

In the elemental approach the spatial integrals in Equation (A.37) are replaced by summations over the uniform grid of panel elements. According to the notations defined in Section A.1.2, this gives

$$P(\omega) = \frac{\omega^2 \rho_0}{4\pi c_0} \sum_{i=1}^{N_e} \sum_{j=1}^{Ne} \frac{\sin(kR_{i,j})}{kR_{i,j}} \, \tilde{\dot{w}}^*(x_i, y_i, \omega) \, \tilde{\dot{w}}(x_j', y_j, ' \omega), \tag{A.41}$$

which can be casted in the following matrix expression

$$\begin{aligned} P(\omega) &= \begin{bmatrix} \tilde{\dot{w}}_1^* & \cdots & \tilde{\dot{w}}_{N_e}^* \end{bmatrix} \begin{bmatrix} R_{rad_{1,1}} & \cdots & R_{rad_{1,N_e}} \\ \vdots & \ddots & \vdots \\ R_{rad_{N_e,1}} & \cdots & R_{rad_{N_e,N_e}} \end{bmatrix} \begin{bmatrix} \tilde{\dot{w}}_1 \\ \vdots \\ \tilde{\dot{w}}_{N_e} \end{bmatrix} \\ &= \tilde{\dot{\mathbf{w}}}_e^H \, \mathbf{R}_{rad} \, \tilde{\dot{\mathbf{w}}}_e. \end{aligned} \tag{A.42}$$

In this equation $\tilde{\dot{\mathbf{w}}}_e$ denotes the vector of element velocities given in Equation (A.17) and $\mathbf{R}_{rad}$ denotes the element radiation matrix with the elements $R_{rad_{i,j}}(\omega)$ given by [3]:

$$R_{rad_{i,j}}(\omega) = \frac{\omega^2 \rho_0 A_e^2}{4\pi c_0} \frac{\sin(k_0 R_{i,j})}{k_0 R_{i,j}}, \tag{A.43}$$

where the diagonal terms of the radiation matrix $R_{i,i}(\omega)$ reduce to

$$R_{rad_{i,i}}(\omega) = \frac{\omega^2 \rho_0 A_e^2}{4\pi c_0}. \tag{A.44}$$

Note that the radiation matrix is proportional to the real part of the radiation resistance matrix, i.e proportional to the real part of the radiation impedance matrix

$$\mathbf{R}_{rad}(\omega) = \frac{A_e}{2} Re\left\{\tilde{\mathbf{Z}}_{rad}\right\}, \tag{A.45}$$

where the terms in the elemental radiation impedance matrix $\tilde{\mathbf{Z}}_{rad}$ are given by

$$\tilde{Z}_{rad_{i,j}}(\omega) = \frac{j\omega\rho_0 A_e}{2\pi} \frac{e^{-jk_0 R_{i,j}}}{R_{i,j}}. \tag{A.46}$$

A.4 Power spectral density of total kinetic energy

It can be demonstrated [35] (page 58), that the power spectral density of $x(t)$ is given by

$$S_{xx}(\omega) = \lim_{T\to\infty} E\left[\frac{1}{T}\,\tilde{x}^*(\omega)\tilde{x}(\omega)\right], \tag{A.47}$$

where $\tilde{x}(\omega)$ is the finite Fourier transform of $x(t)$:

$$\tilde{x}(\omega) = \frac{1}{2\pi}\int_0^T x(t)e^{-j\omega t}\,dt \tag{A.48}$$

and $E[\ ]$ denotes the expectation for and infinite sample length. Thus considering the general formulation for the instantaneous total kinetic energy in Equation (A.21), the power spectral density of the total kinetic energy S_E, due to a time and spatial stochastic disturbance over the panel surface, can be written as [33]:

$$S_E(\omega) = \frac{1}{2}\int_0^{l_x}\int_0^{l_y} \rho h \lim_{T\to\infty} E\left[\frac{1}{T}\,\tilde{\dot{w}}^*(x,y,\omega)\tilde{\dot{w}}(x,y,\omega)\right] dx\,dy. \tag{A.49}$$

A.4.1 Modal formulation

Substituting the modal expression for the transverse velocity of Equation (A.4), into Equation (A.49) gives

$$\begin{aligned} S_E(\omega) &= \frac{1}{2}\int_0^{l_x}\int_0^{l_y} \rho h \lim_{T\to\infty} E\left[\frac{1}{T}\sum_{r=1}^{\infty}\phi_r(x,y)\tilde{\dot{a}}_r^*(\omega)\sum_{s=1}^{\infty}\phi_s(x,y)\tilde{\dot{a}}_s(\omega)\right] dx\,dy \\ &= \frac{1}{2}\int_0^{l_x}\int_0^{l_y} \rho h \sum_{r=1}^{\infty}\sum_{s=1}^{\infty}\phi_r(x,y)\phi_s(x,y) \lim_{T\to\infty} E\left[\frac{1}{T}\,\tilde{\dot{a}}_r^*(\omega)\tilde{\dot{a}}_s(\omega)\right] dx\,dy. \end{aligned} \tag{A.50}$$

Assuming ρh=constant and considering the orthogonality conditions in Equations (A.27) and (A.28), Equation (A.50) results in

$$
\begin{aligned}
S_E(\omega) &= \frac{1}{2}\,\rho h \sum_{r=1}^{\infty}\sum_{s=1}^{\infty}\int_0^{l_x}\int_0^{l_y}\phi_r(x,y)\phi_s(x,y)S_{a_r a_s}dx\,dy \\
&= \frac{1}{2}\,\rho h \sum_{r=1}^{\infty}\int_0^{l_x}\int_0^{l_y}\phi_r(x,y)^2 dx\,dy\,S_{a_r a_r} \\
&= \frac{M}{2}\sum_{r=1}^{\infty}S_{a_r a_r}, \qquad \text{(A.51)}
\end{aligned}
$$

where $S_{a_r a_r}$ is the power spectral density of modal velocities and M is the mass of the panel. According to Equation (A.47) the power spectral density of modal velocities can be expressed as

$$
S_{a_r a_r}(\omega) = \lim_{T\to\infty} E\left[\frac{1}{T}\,\tilde{\dot{a}}_r^*(\omega)\tilde{\dot{a}}_r(\omega)\right] = \lim_{T\to\infty} E\left[\frac{1}{T}\,\left|\tilde{\dot{a}}_r(\omega)\right|^2\right]. \qquad \text{(A.52)}
$$

Substituting Equation (A.5) into this expression gives

$$
\begin{aligned}
S_{a_r a_r}(\omega) &= \lim_{T\to\infty} E\left[\frac{1}{T}\,\tilde{\Omega}_r^*(\omega)\tilde{F}_r^*(\omega)\tilde{\Omega}_r(\omega)\tilde{F}_r(\omega)\right] \\
&= \lim_{T\to\infty} E\left[\frac{1}{T}\,\left|\tilde{\Omega}_r(\omega)\right|^2\tilde{F}_r^*(\omega)\tilde{F}_r(\omega)\right] \\
&= \left|\tilde{\Omega}_r(\omega)\right|^2 \lim_{T\to\infty} E\left[\frac{1}{T}\,\tilde{F}_r^*(\omega)\tilde{F}_r(\omega)\right] \qquad \text{(A.53)}
\end{aligned}
$$

.

Substituting the formulation for the modal excitation terms in Equation (A.9) then gives

$$
\begin{aligned}
S_{a_r a_r}(\omega) &= \left|\tilde{\Omega}_r(\omega)\right|^2 \lim_{T\to\infty} E\left[\frac{1}{T}\int_0^{l_x}\int_0^{l_y}\phi_r(x,y)\,\tilde{f}^*(x,y,\omega)\,dx\,dy\int_0^{l_x}\int_0^{l_y}\phi_r(x',y')\,\tilde{f}(x',y',\omega)\,dx'\,dy'\right] \\
&= \left|\tilde{\Omega}_r(\omega)\right|^2 \int_0^{l_x}\int_0^{l_y}\int_0^{l_x}\int_0^{l_y}\phi_r(x,y)\,\phi_r(x',y') \lim_{T\to\infty} E\left[\frac{1}{T}\,\tilde{f}^*(x,y,\omega)\,\tilde{f}(x',y',\omega)\right]dx\,dy\,dx'\,dy' \\
&= \left|\tilde{\Omega}_r(\omega)\right|^2 \int_0^{l_x}\int_0^{l_y}\int_0^{l_x}\int_0^{l_y}\phi_r(x,y)\,\phi_r(x',y')\,\tilde{S}_{ff}(x,y,x',y',\omega)dx\,dy\,dx'\,dy', \qquad \text{(A.54)}
\end{aligned}
$$

where $\tilde{S}_{ff}(x, y, x', y', \omega)$ is the cross spectral density of the stochastic disturbance per unit area between positions (x, y) and (x', y'), which can be expressed as the product of the power spectral density $\Psi(\omega)$ and the spatial correlation function $\tilde{C}(x, y, x', y', \omega)$ of the disturbance so that

$$\tilde{S}_{ff}(x, y, x', y', \omega) = \Psi(\omega)\, \tilde{C}(x, y, x', y', \omega). \tag{A.55}$$

Both power spectral density $\Psi(\omega)$ and spatial correlation function $\tilde{C}(x, y, x', y', \omega)$ are specific properties of the disturbance. Formulations that describe the the spatial correlation functions for ADF and TBL excitation are given in section 3.2. Substituting Equation (A.54) back into Equation (A.50) gives the final expression for the power spectral density of total kinetic energy due to a time and spatial stochastic disturbance as

$$S_E(\omega) = \frac{M}{2} \sum_{r=1}^{\infty} \left| \tilde{\Omega}_r(\omega) \right|^2 \int_0^{l_x} \int_0^{l_y} \int_0^{l_x} \int_0^{l_y} \phi_r(x, y)\, \phi_r(x', y')\, \tilde{S}_{ff}(x, y, x', y', \omega) dx\, dy\, dx'\, dy'. \tag{A.56}$$

A.4.2 Elemental approach

According to the notations in section A.1.2, the spatial integral in Equation (A.49) can be replaced by a summation of element contributions, so that the power spectral density of the total kinetic energy due to time and spatial stochastic disturbances is given by

$$S_E(\omega) = \frac{1}{2} \sum_{i=1}^{N_e} \rho h\, A_e \lim_{T \to \infty} E\left[\frac{1}{T}\, \tilde{\tilde{w}}^*(x_i, y_i, \omega)\, \tilde{\tilde{w}}(x_i, y_i, \omega) \right] \tag{A.57}$$

where A_e denotes the area of a single panel element and $\tilde{\tilde{w}}(x_i, y_i, \omega)$ is the transverse velocity of the i-th element. Using the vector formulation for the elemental velocities given in Equation (A.18) the expression for the power spectral density becomes

$$
\begin{aligned}
S_E(\omega) &= \frac{M_e}{2} \sum_{i=1}^{N_e} \lim_{T\to\infty} E\left[\frac{1}{T}\,\hat{\dot{w}}_i^*(\omega)\,\hat{\dot{w}}_i(\omega)\right] \\
&= \frac{M_e}{2}\, trace\left(\lim_{T\to\infty} E\left[\frac{1}{T}\begin{bmatrix}\tilde{\dot{w}}_1\\ \vdots \\ \tilde{\dot{w}}_{N_e}\end{bmatrix}\begin{bmatrix}\tilde{\dot{w}}_1^* & \cdots & \tilde{\dot{w}}_{N_e}^*\end{bmatrix}\right]\right) \\
&= \frac{M_e}{2}\, trace\left(\lim_{T\to\infty} E\left[\frac{1}{T}\left[\tilde{\dot{\mathbf{w}}}_e \tilde{\dot{\mathbf{w}}}_e^H\right]\right]\right) \\
&= \frac{M_e}{2}\, trace\left(\lim_{T\to\infty} E\left[\frac{1}{T}\left[\mathbf{\Phi}_e \tilde{\dot{\mathbf{a}}}\,\tilde{\dot{\mathbf{a}}}^H \mathbf{\Phi}_e^T\right]\right]\right) \\
&= \frac{M_e}{2}\, trace\left(\mathbf{\Phi}_e \lim_{T\to\infty} E\left[\frac{1}{T}\left[\tilde{\dot{\mathbf{a}}}\,\tilde{\dot{\mathbf{a}}}^H\right]\right]\mathbf{\Phi}_e^T\right) \\
&= \frac{M_e}{2}\, trace\left(\mathbf{\Phi}_e \tilde{\mathbf{S}}_{\dot{a}\dot{a}}(\omega)\mathbf{\Phi}_e^T\right), \qquad \text{(A.58)}
\end{aligned}
$$

where $\tilde{\mathbf{S}}_{\dot{a}\dot{a}}(\omega)$ is the $[N \times N]$ dimensional matrix of power and cross spectral densities of the modal velocities. According to Equation (A.18) the vector of modal velocities is given by

$$
\tilde{\dot{\mathbf{a}}} = \tilde{\mathbf{\Omega}}\mathbf{\Phi}_e^T \tilde{\mathbf{F}}_e, \qquad \text{(A.59)}
$$

thus $\tilde{\mathbf{S}}_{\dot{a}\dot{a}}(\omega)$ can be written as

$$
\begin{aligned}
\tilde{\mathbf{S}}_{\dot{a}\dot{a}}(\omega) &= \lim_{T\to\infty} E\left[\frac{1}{T}\left[\tilde{\dot{\mathbf{a}}}\,\tilde{\dot{\mathbf{a}}}^H\right]\right] \\
&= \lim_{T\to\infty} E\left[\frac{1}{T}\,\tilde{\mathbf{\Omega}}^H \mathbf{\Phi}_e^T \tilde{\mathbf{F}}_e \tilde{\mathbf{F}}_e^H \mathbf{\Phi}_e \tilde{\mathbf{\Omega}}\right] \\
&= \tilde{\mathbf{\Omega}}\mathbf{\Phi}_e^T \lim_{T\to\infty} E\left[\frac{1}{T}\,\tilde{\mathbf{F}}_e \tilde{\mathbf{F}}_e^H\right]\mathbf{\Phi}_e \tilde{\mathbf{\Omega}}^H \\
&= \tilde{\mathbf{\Omega}}\,\mathbf{\Phi}_e^T\,\tilde{\mathbf{S}}_{f_e f_e}(\omega)\,\mathbf{\Phi}_e\,\tilde{\mathbf{\Omega}}^H, \qquad \text{(A.60)}
\end{aligned}
$$

where $\tilde{\mathbf{S}}_{f_e f_e}(\omega)$ is the $[N_e \times N_e]$ dimensional matrix with the power and cross spectral densities of the element excitation forces, which has the form

$$\tilde{\mathbf{S}}_{f_e f_e} = \begin{bmatrix} S_{f_1,f_1} & \cdots & \tilde{S}_{f_1,f_{N_e}} \\ \vdots & \ddots & \vdots \\ \tilde{S}_{f_{N_e},f_1} & \cdots & S_{f_{N_e},f_{N_e}} \end{bmatrix} \tag{A.61}$$

with the elements

$$\tilde{S}_{f_i f_j}(\omega) = A_e^2 \; \tilde{S}_{ff}\left(x_i, y_i, x_j, y_j, \omega\right), \tag{A.62}$$

where A_e is the surface of a single element and $\tilde{S}_{ff}\left(x_i, y_i, x_j, y_j, \omega\right)$ is the cross spectral density of the stochastic disturbance in Equation (A.55), evaluated for the centres of element i and j. Substituting the final expression in Equation (A.60) back into the Equation (A.58) gives

$$\begin{aligned} S_E(\omega) &= \frac{M_e}{2} \, trace\left(\mathbf{\Phi}_e \, \tilde{\mathbf{\Omega}} \, \mathbf{\Phi}_e^T \, \tilde{\mathbf{S}}_{f_e f_e}(\omega) \, \mathbf{\Phi}_e \, \tilde{\mathbf{\Omega}}^H \, \mathbf{\Phi}_e \right) \\ &= \frac{M_e}{2} \, trace\left(\tilde{\mathbf{Y}}_{ee} \tilde{\mathbf{S}}_{f_e f_e}(\omega) \tilde{\mathbf{Y}}_{ee}^H\right), \end{aligned} \tag{A.63}$$

where $\tilde{\mathbf{Y}}_{ee} = \mathbf{\Phi}_e \tilde{\mathbf{\Omega}} \mathbf{\Phi}_e^T$ is the $[N_e \times N_e]$ dimensional matrix of element point and transfer mobilities.

A.5 Power spectral density of total sound power radiated

Considering the general formulation for the instantaneous total radiated sound power given in Equation (A.33) and considering the relationship for the spectral density given in Equation (A.47), the power spectral density of the total sound power radiated due to time and spatial stochastic disturbances given by

$$S_P(\omega) = Re\left\{ \int_0^{l_x} \int_0^{l_y} \lim_{T \to \infty} E\left[\frac{1}{T} \, \tilde{\dot{w}}^*(x, y, \omega) \tilde{p}(x, y, 0, \omega) \right] dx \, dy \right\}. \tag{A.64}$$

Substituting the Rayleigh integral expression for $\tilde{p}(x, y, 0, \omega)$ from Equation (A.36) gives

$$S_P(\omega) = Re\left\{ \frac{j\omega\rho_0}{2\pi} \int_0^{l_x}\int_0^{l_y}\int_0^{l_x}\int_0^{l_y} \frac{e^{-jk_0R}}{R} \lim_{T\to\infty} E\left[\frac{1}{T}\,\tilde{w}^*(x,y,\omega)\tilde{w}(x',y',\omega)\right] dx\,dy\,dx'\,dy' \right\}. \quad \text{(A.65)}$$

A.5.1 Modal formulation

Substituting the modal expression for the transverse velocity of Equation (A.4) into Equation (A.65) gives

$$\begin{aligned} S_P(\omega) &= Re\left\{ \frac{j\omega\rho_0}{2\pi} \int_0^{l_x}\int_0^{l_y}\int_0^{l_x}\int_0^{l_y} \frac{e^{-jk_0R}}{R} \lim_{T\to\infty} E\left[\frac{1}{T}\sum_{r=1}^{\infty}\phi_r(x,y)\tilde{\dot{a}}_r^*(\omega)\sum_{s=1}^{\infty}\phi_s(x',y')\tilde{\dot{a}}_s(\omega)\right] dx\,dy\,dx'\,dy' \right\} \\ &= Re\left\{ \frac{j\omega\rho_0}{2\pi} \int_0^{l_x}\int_0^{l_y}\int_0^{l_x}\int_0^{l_y} \sum_{r=1}^{\infty}\sum_{s=1}^{\infty}\phi_r(x,y)\frac{e^{-jk_0R}}{R}\,\phi_s(x',y') \lim_{T\to\infty} E\left[\frac{1}{T}\,\tilde{\dot{a}}_r^*(\omega)\tilde{\dot{a}}_s(\omega),\right] dx\,dy\,dx'\,dy' \right\} \\ &= \sum_{r=1}^{\infty}\sum_{s=1}^{\infty} Re\left\{ \frac{j\omega\rho_0}{2\pi} \int_0^{l_x}\int_0^{l_y}\int_0^{l_x}\int_0^{l_y} \phi_r(x,y)\,\frac{e^{-jk_0R}}{R}\,\phi_s(x',y')\,\tilde{S}_{a_ra_s} dx\,dy\,dx'\,dy' \right\}, \end{aligned} \quad \text{(A.66)}$$

where $\tilde{S}_{a_ra_s}$ is the spectral density of the the modal velocities. Substituting the formulation for the modal velocities of Equation (A.5) gives

$$\begin{aligned} S_{a_ra_s}(\omega) &= \lim_{T\to\infty} E\left[\frac{1}{T}\,\tilde{\dot{a}}_r^*(\omega)\tilde{\dot{a}}_s(\omega)\right] \\ &= \lim_{T\to\infty} E\left[\frac{1}{T}\,\tilde{\Omega}_r^*(\omega)\tilde{F}_r^*(\omega)\tilde{\Omega}_s(\omega)\tilde{F}_s(\omega)\right] \\ &= \tilde{\Omega}_r(\omega)\tilde{\Omega}_s^*(\omega) \lim_{T\to\infty} E\left[\frac{1}{T}\,\tilde{F}_r^*(\omega)\tilde{F}_s(\omega)\right]. \end{aligned} \quad \text{(A.67)}$$

Substituting the formulation for the modal excitation terms in Equation (A.9) then gives

$$
\begin{aligned}
S_{a_r a_s}(\omega) &= \tilde{\Omega}_r(\omega)\tilde{\Omega}_s^*(\omega) \lim_{T\to\infty} E\left[\frac{1}{T}\int_0^{l_x}\int_0^{l_y} \phi_r(x,y)\,\tilde{f}^*(x,y,\omega)\,dx\,dy \int_0^{l_x}\int_0^{l_y} \phi_s(x',y')\,\tilde{f}(x',y',\omega)\,dx'\,dy'\right] \\
&= \tilde{\Omega}_r(\omega)\tilde{\Omega}_s^*(\omega) \int_0^{l_x}\int_0^{l_y}\int_0^{l_x}\int_0^{l_y} \phi_r(x,y)\,\phi_s(x',y') \lim_{T\to\infty} E\left[\frac{1}{T}\,\tilde{f}^*(x,y,\omega)\,\tilde{f}(x',y',\omega)\right] dx\,dy\,dx'\,dy' \\
&= \tilde{\Omega}_r(\omega)\tilde{\Omega}_s^*(\omega) \int_0^{l_x}\int_0^{l_y}\int_0^{l_x}\int_0^{l_y} \phi_r(x,y)\,\phi_s(x',y')\,\tilde{S}_{ff}(x,y,x',y',\omega)dx\,dy\,dx'\,dy'. \qquad \text{(A.68)}
\end{aligned}
$$

Finally, substituting this formulation for spectral density of the the modal velocities back in to Equation (A.66) gives

$$
\begin{aligned}
S_P(\omega) &= \sum_{r=1}^{N}\sum_{s=1}^{N} \tilde{\Omega}_r(\omega)\tilde{\Omega}_s^*(\omega) \\
&\quad \times Re\left\{\frac{j\omega\rho_0}{2\pi}\int_0^{l_x}\int_0^{l_y}\int_0^{l_x}\int_0^{l_y} \phi_r(x,y)\,\frac{e^{-jk_0R}}{R}\,\phi_s(x',y')\,dx\,dy\,dx'\,dy'\right. \\
&\quad \left.\times \int_0^{l_x}\int_0^{l_y}\int_0^{l_x}\int_0^{l_y} \phi_r(x,y)\,\phi_s(x',y')\,\tilde{S}_{ff}(x,y,x',y',\omega)\,dx\,dy\,dx'\,dy'\right\}. \qquad \text{(A.69)}
\end{aligned}
$$

A.5.2 Elemental approach

Substituting the spatial integrals in Equation (A.65) by a finite summation over all panel elements gives the following expression for the power spectral density of the total sound power radiated due to time and spatial stochastic disturbances:

$$
\begin{aligned}
S_P(\omega) &= Re\left\{\frac{j\omega\rho_0 A_e^2}{2\pi}\sum_{i=1}^{N_e}\sum_{j=1}^{N_e}\frac{e^{-jkR_{i,j}}}{R_{i,j}}\lim_{T\to\infty}E\left[\frac{1}{T}\,\tilde{\dot{w}}^*(x_i,y_i,\omega)\,\tilde{\dot{w}}(x_i,y_i,\omega)\right]\right\} \\
&= 2\lim_{T\to\infty}E\left[\frac{1}{T}\left[\begin{array}{ccc}\tilde{\dot{w}}_1^* & \cdots & \tilde{\dot{w}}_{N_e}^*\end{array}\right]\left[\begin{array}{ccc}R_{rad_{1,1}} & \cdots & R_{rad_{1,N_e}}\\ \vdots & \ddots & \vdots \\ R_{rad_{N_e,1}} & \cdots & R_{rad_{N_e,N_e}}\end{array}\right]\left[\begin{array}{c}\tilde{\dot{w}}_1\\ \vdots\\ \tilde{\dot{w}}_{N_e}\end{array}\right]\right] \\
&= 2\lim_{T\to\infty}E\left[\frac{1}{T}\,\tilde{\dot{\mathbf{w}}}_e^H\,\mathbf{R}_{rad}\,\tilde{\dot{\mathbf{w}}}_e\right], \qquad \text{(A.70)}
\end{aligned}
$$

where $\mathbf{R}_{rad}$ is the elemental radiation impedance matrix as defined in Equations (A.43) to (A.46). Equation (A.70) can be rewritten to give

$$
\begin{aligned}
S_P(\omega) &= 2\,trace\left(\lim_{T\to\infty}E\left[\frac{1}{T}\,\tilde{\dot{\mathbf{w}}}_e\,\tilde{\dot{\mathbf{w}}}_e^H\,\mathbf{R}_{rad}\right]\right) \\
&= 2\,trace\left(\lim_{T\to\infty}E\left[\frac{1}{T}\,\mathbf{\Phi}_e\,\tilde{\dot{\mathbf{a}}}\tilde{\dot{\mathbf{a}}}^H\mathbf{\Phi}_e^T\,\mathbf{R}_{rad}\right]\right) \\
&= 2\,trace\left(\mathbf{\Phi}_e\,\tilde{\mathbf{S}}_{\dot{a}\dot{a}}\mathbf{\Phi}_e^T\,\mathbf{R}_{rad}\right), \qquad \text{(A.71)}
\end{aligned}
$$

where the $[N\times N]$ dimentional matrix of power and cross spectral densities of the modal velocities $\tilde{\mathbf{S}}_{\dot{a}\dot{a}}$ is derived in Equation (A.60), so that:

$$
\begin{aligned}
S_P(\omega) &= 2\,trace\left(\left[\mathbf{\Phi}_e\,\tilde{\mathbf{\Omega}}\,\mathbf{\Phi}_e^T\,\tilde{\mathbf{S}}_{f_ef_e}\,\mathbf{\Phi}_e\,\tilde{\mathbf{\Omega}}^H\,\mathbf{\Phi}_{e,r}^T\right]\mathbf{R}_{rad}\right) \\
&= 2\,trace\left(\left[\tilde{\mathbf{Y}}_{ee}\,\tilde{\mathbf{S}}_{f_ef_e}\,\tilde{\mathbf{Y}}_{ee}^H\right]\mathbf{R}_{rad}\right), \qquad \text{(A.72)}
\end{aligned}
$$

where $\tilde{\mathbf{Y}}_{ee}$ is the $[N_e\times N_e]$ dimensional matrix of the element point and transfer mobilities and $\tilde{\mathbf{S}}_{f_ef_e}$ is the matrix with the power and cross spectral densities of the element excitation forces given in Equation (A.61).